Chapter 8

Network Coding-Assisted Retransmission Scheme for Video-Streaming Services over Wireless Access Networks

Aleš Švigelj and Melisa Junuzović

Additional information is available at the end of the chapter

http://dx.doi.org/10.5772/intechopen.71784

Abstract

Video-streaming services, such as Internet protocol television, promising the delivery of multimedia contents over wireless access networks to clients whenever and wherever, are becoming more and more popular. However, scarce radio resources, lossy characteristics of wireless links and high bandwidth demands pose the never-ending challenges for provisioning of real-time streaming services over wireless networks in a timely and reliable manner. Furthermore, a wireless channel may suffer from interference and multipath fading, which may cause random packet losses. In addition, wireless link layer does not provide a retransmission mechanism for multicast/broadcast traffic. This would significantly impact the clients' quality of experience of streaming services. Traditional unicast retransmission solutions improve client's quality, at the bandwidth expense, because every lost packet must be retransmitted separately. This chapter presents and practically evaluates a retransmission scheme for video-streaming services over last mile wireless networks. It is based on network coding techniques that increase the overall performance by means of reducing the number of physical transmissions, in comparison to traditional unicast retransmission approach, resulting in reduced bandwidth consumption. Thus, the Internet service providers can increase the number of clients over the same infrastructure or, alternatively, offer more services to the clients.

Keywords: retransmission, wireless network, broadcast, network coding, streaming, IPTV

1. Introduction

The provision and efficient delivery of high-quality real-time streaming services, such as Internet protocol television (IPTV) over wireless networks (e.g., Wi-Fi) in the last mile, introduces never-ending challenges. Easy and fast deployment and relatively low deployment costs

of Wireless IEEE 802.11 networks, where one antenna covers several different clients/groups of clients, stimulate the usage of Wi-Fi technology in underdeveloped countries and rural areas. However, the bottleneck in the content delivery is due to spectrum limitations in wireless medium shifted to the last mile. Thus for ISPs, it is of paramount importance to increase the last mile access performance as in such cases, the bandwidth reduction means better services for existing clients, or alternatively, additional clients over the same infrastructure. Thus in this chapter, we are addressing the efficient and quality delivery of video-streaming services such as IPTV using the IEEE 802.11 wireless broadcast network in the last mile [1].

By using IEEE 802.11 wireless network in the last mile, the video content can be delivered using unicast or broadcast/multicast mechanism. Due to the fact that unicast mechanism, which delivers the content to clients individually and supports retransmissions (and back off) that assure reliable content delivery, is a preferred solution in currently deployed systems. On the other hand, multicasting can be used instead of unicasting in order to reduce the bandwidth. The bandwidth can be significantly reduced in particular, when multiple clients watch the same video stream, as the server, instead of sending multiple packets to different clients, has to send only one packet. All broadcast packets are delivered to all clients only under ideal wireless channel conditions. However, the packet losses frequently occur in the practical wireless environment; thus, some sort of retransmission mechanism is necessary to ensure reliability. In order to support reliability and/or reduce bandwidth consumption, different retransmission schemes have been proposed, where some of them also consider network coding (NC).

Since the pioneering work in network coding [2], numerous papers appeared on this subject and significant progress has been made in applying NC to different networks. NC has already been successfully used to increase throughput as shown in practical deployment in [3], where a reliable and scalable live streaming solution is presented. It is based on wireless multicast with real-time network coding in hyper-dense Wi-Fi spaces. A timely delivery scheme that uses a minimum amount of feedback from the clients is at the core of this approach. It generates coded repair packets, which are useful to a large number of clients. Packet loss estimation is used in the scheme, which is able to operate well with a very limited amount of feedback. Besides, all coded packets are linear combinations of original packets over the Galois field of size 2. Nevertheless, they are focusing on satisfying different clients' requests regarding the same flow, while we are focusing on satisfying different clients regarding different flows, using different approach of NC and feedbacks.

In [4], for the particular case of wireless mesh network, a network coding and scheduling scheme for transmitting several video streams over a wireless mesh network is proposed. Their main outcome is that in a network coding capable wireless network, the transmission of video streams should be optimized also, and even more important than for network throughput, for video quality. All approaches mentioned in [4–6] are designed for intersession network coding, by combining different flows. They compute a packet that must be decoded by the next hop of the head of the sender's output queue, based on a first in first out (FIFO) management for the requests of each client. However, there is no such restriction in our proposal and all client requests are taken into consideration, which significantly changes the complexity and the nature of the coding problem.

http://dx.doi.org/10.5772/intechopen.71784

Retransmission schemes based on NC are discussed in [7–9]. Their key idea, in order to combine different lost packets with network coding to achieve retransmission, is to use the feedback of lost packets information. Their approaches by broadcasting combined packets effectively save the number of transmissions and advance the efficiency of transmissions. However, in practical real-time streaming applications, those approaches have their own drawbacks and limitations.

Depending on the NC application, the implementation affects different open systems interconnection (OSI) layers. In this chapter, we propose transmission scheme that is integrated in the application layer and is adapted for video-streaming applications such as IPTV. It can be used for increasing network throughput of mobile and static wireless networks. We also evaluate its performance using practical Wi-Fi test bed that comprises a streaming server and multiple Wi-Fi clients.

The rest of the chapter is organized as follows. In this section, we introduced the video-streaming challenges in wireless medium using IPTV. Section 2 discusses the packet loss recovery techniques in streaming wireless networks. Section 3 proposes concept of transmission scheme for reliable video-streaming service using network coding and gives an overview about implementation details. Practical evaluation of the proposed solutions is described in Section 4, and finally, Section 5 concludes the chapter.

1.1. Wireless medium challenges

The main advantages of wireless networks over wired counterparts include ease of deployment and mobile clients support. However, the unique characteristics of video data amplify the difficulty of video transmission and thus impose a number of challenges. Some of the main challenges of wireless networking and their impact on video communication are discussed and highlighted in the following.

- Shadowing and multipath fading: they are common wireless effects. Shadowing is caused by obstacles between the transmitter and the receiver that attenuate signal power through absorption, reflection, scattering, and diffraction. It occurs over a relatively large time scale. On the other hand, multipath fading is due to multipath propagation: different path signals are added constructively or destructively. Multipath fading results in rapid fluctuation of signal amplitude within the order of a wavelength. The presence of shadowing and multipath fading results in time-varying channel conditions and location-dependent packet erasures. They cause burst errors in the form of multiple lost packets.
- Limited bandwidth: wireless networks are limited in capacity. Although, the 802.11 products are advertised as having a high data rate. Still, “protection” mechanisms such as binary exponential back off, rate adaptation, and protocol overheads cut the throughput by 50% or more. Moreover, due to the shared nature of the wireless medium, the actual bandwidth available to individual clients can even be much lower, posing a great obstacle for providing high bandwidth video services.
- Interference: wireless medium is shared among multiple clients; thus signals, which arrive at a receiver from other concurrent transmissions, although attenuated, cause the

interference for the receiver. It is a common effect in WLANs because they operate in the unlicensed 2.4/5 GHz industrial, scientific, and medical (ISM) frequency band. Interference affects the quality of a wireless link, and consequently, its error rate and achievable capacity.

1.2. Video-streaming challenges

Video services and applications have become the driving force in the development and widespread deployment of wireless broadband access technologies and high speed local area networks. Convenient and cable-free connectivity can be achieved by using wireless local area networking (WLAN) technologies. Using the wireless networks, it also can provide mobility to portable TVs.

As conventional service architectures, network structures and protocols have not been designed to consider the high data rate and real-time transmission requirements of digital video, they lack to provide a robust medium distribution.

Video-streaming applications have distinctive QoS requirements, such as high bandwidth requirement, delay sensitiveness, and loss tolerance. We list the challenging QoS issues as follows:

- Bandwidth: transmission of video sequences typically has a minimum bandwidth requirement in order to achieve acceptable presentation quality. Therefore, supporting the delivery of video over time-varying wireless links could be very unreliable. The challenge lies in keeping the quality degradation to a level that is hardly noticeable or tolerable while utilizing the wireless resources efficiently.
- Delay: in contrast to data transmission, which is usually not subjected to strict delay constraints, video-streaming requires bounded end-to-end delay. Each video frame needs to arrive at the client to be decoded and displayed, before its play out deadline. Otherwise, it is useless. If the video packet does not arrive on time, the play out process will have to be temporally paused, which is annoying to human eyes and deteriorates the overall streaming quality. Consequently, video-streaming applications are usually known to be very sensitive to delay.
- Packet loss: video-streaming technology is tolerant to a certain level of loss, since the visual quality will still be acceptable if the packet loss ratio is kept below a certain threshold. However, loss of packets can potentially make the presentation displeasing to human eyes, especially when some of the key video frames are lost, which could make the presentation impossible.
- Unreliability: Wi-Fi does not provide a retransmission mechanism for broadcast/multicast transmissions (with multiple clients). Wi-Fi multicast traffic could normally experience a packet loss rate of 5%. As a loss of even a single video packet can result as an error that propagates for many video frames, this is a serious problem. Thus, it is quite normal that multicast video applications fail completely when they operate on a Wi-Fi network although they work fine on a wired network.

http://dx.doi.org/10.5772/intechopen.71784

1.3. IPTV

Internet protocol television (IPTV) is a system that is used to deliver the Internet television services across the Internet protocol (IP) infrastructure. IPTV integrates voice, video, and data delivery into a single IP framework, to enable interactive broadcasting services to the subscribers. It promises significant advantages for both service providers and clients.

In the past few years, IPTV has gained an unremarkable growth rate. IPTV services are becoming very popular among telecommunication companies, most of all because they can provide television programs anytime and anywhere. IPTV can support broadcast and unicast services, such as broadcasting of TV channels, Video on demand (VoD) or time-shifted television. Unlike conventional broadcasting systems, IPTV broadcasts will not be restricted by the limited number of channels in the broadcast/radio spectrum.

Besides, IPTV will provide its clients with the opportunity to access and interact with a wide variety of high quality on demand video content over the Internet. Since IPTV is considered as a real-time broadcast service over the Internet, the success of the IPTV service depends on the quality of experience (QoE) perceived by the end clients.

The IPTV system has to support a wide range of transmission channel characteristics (i.e., varying packet loss rates and transmission delays) between the content providers and the end clients. The characteristics of video traffic as well as the high-quality requirements of IPTV broadcast impose strict requirements on transmission delay. IPTV framework has to provide mechanisms to satisfy the stringent delay, jitter, and bandwidth requirements over lossy transmission channels.

The architecture of IPTV is composed of five main parts as depicted in **Figure 1**: (i) head network, (ii) core network, (iii) distribution network, (iv) access network, and (v) customer network.

Transport network includes the core network, distribution network, and access network. IPTV service provider transports the IPTV streams to client end by using all entities of the transport

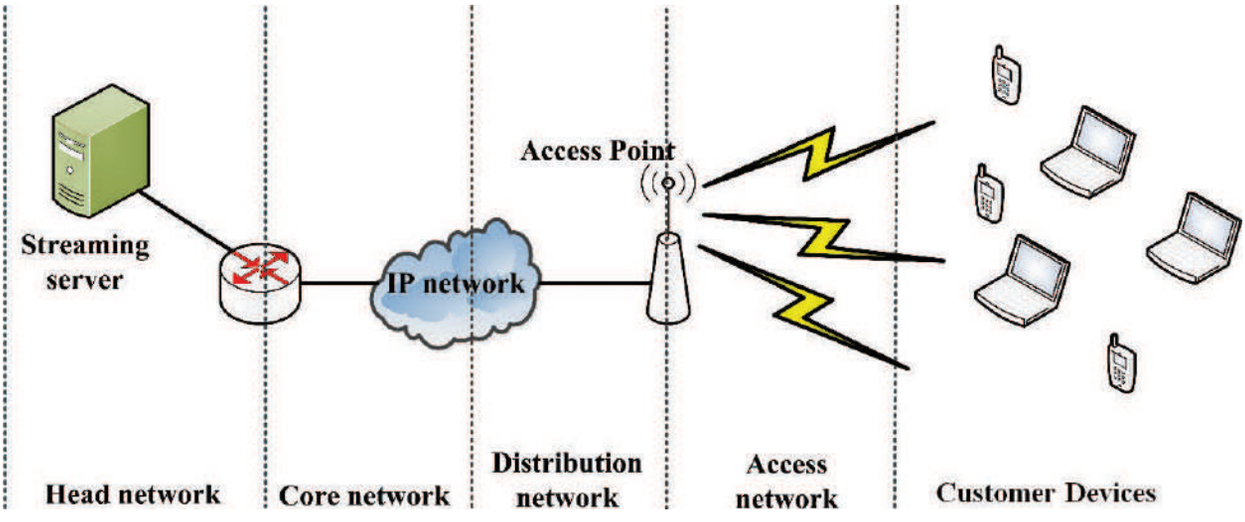

Figure 1. IPTV architecture.

network. Among all these entities, major bandwidth restricting entity in transport network is the access point (AP) because of limited buffer size of queues. To avoid bandwidth restriction, wired access links such as cable and digital subscriber line (DSL) are preferred by IPTV service providers.

Using WLAN for IPTV distribution improves the mobility and flexibility of IPTV network deployment; however, it has its challenges as described in previous sections and it can impact the clients' quality of experience when watching an IPTV program.

Error correction schemes such as forward error correction (FEC) and/or retransmissions can be used to improve reliability of an IPTV program. Both of them are explained in more detail below.

2. Packet loss recovery

Considering the earlier mentioned strict quality requirements of video, strong error recovery techniques are required to protect the content that is delivered to end clients and recover from the occasional packet losses. As it can be seen from the previous examples, there are two possibilities either to prevent packet loss or, alternatively, when packet loss does happen, reduce the noticeable effects of packet loss or restore the missing packets.

In other words, one wants to provide a mechanism to recover from packet loss or to have an error resiliency mechanism that reduces errors due to packet loss. Numerous techniques for providing error resiliency against packet loss can be divided in two categories:

- Techniques that provide recovery for packet loss.
- Techniques that try to reduce the impact or effect of the packet loss.

Two different techniques aimed to recover packet losses during the delivery of IPTV services are FEC and retransmission. The FEC approach operates by adding redundant information to the data at the server, while the retransmission approach recovers from packet losses by requesting retransmission from the server.

2.1. Forward error correction (FEC)

An FEC-based error recovery protocol uses redundant information to allow the client to correct packet losses. With this redundant information, the clients can recover from packet losses nearby the client. The amount of data that can be reconstructed is determined by the amount of loss and on the amount of redundant data. As an FEC-based recovery mechanism is suitable in networks that only allow unidirectional traffic (e.g., satellite broadcast) or environments where the latency from the client to the server is relatively high (e.g., cellular networks), it does not require any feedback from the server to the client. It can be applied from the physical layer up to the application layer according to the OSI reference model. For IPTV streaming applications, FEC can be offered at network layer, transport layer, or application layer FEC. A disadvantage of a FEC protection mechanism is that the applied FEC protection

scheme might be insufficient (too weak) for certain clients, while at the same time can be superfluous for some other clients, thus being a waste of bandwidth.

2.2. Retransmissions

Packet retransmission is the technique of retransmitting packets that are considered lost. A packet retransmission requires communication between the client and server, as the client needs to explicitly or implicitly request the packet retransmissions from server. The transmission control protocol (TCP) is a well-known protocol using packet retransmission. Bi-directional communication is required at packet retransmission mechanism in order to allow the client to indicate packet loss and to identify which packet needs to be retransmitted. It is typically achieved by applying sequence numbers. To indicate the loss of packets, two types of messages can be used:

- Acknowledgment (ACK) messages can be used to implicitly indicate the loss of a packet by acknowledging the reception of one packet or a sequence of packets. As the missing packet will never be acknowledged, these messages can then be used to implicitly determine packet loss (e.g., TCP uses ACK messages).
- Negative acknowledgment (NACK) messages are used to explicitly indicate that one or more packets were not received. As feedback from client to server is kept to a minimum, NACK messages are used in constrained networks with many clients per server.

A packet retransmission mechanism is adaptive to variable network conditions. When there is no loss in the network, there will be no packet retransmission, hence no additional required bandwidth. Because packet retransmission mechanisms introduce delay, they are only suitable for applications with nonstrict delay requirements.

Using packet retransmissions for (live) IPTV services has also the drawbacks as IPTV streams are not likely to get adapted to congestion. Thus, if congestion occurs during transport, the packet retransmissions may contribute to the network congestion if the packet retransmission is enabled, thus further lowering bandwidth available for IPTV stream delivery.

2.3. Network coding

In the past few years, network coding (NC) has become popular in both wired and wireless networks as a mechanism for increasing the network throughput. Proposed by Ahlswede et al. in [2], it is a technique for increasing the throughput of the network by encoding multiple packets into the same packet, either from the same or from different streams.

Using the NC, the broadcast nature of the wireless medium is exploited. In the wireless physical medium, all data transmitted by the source is in fact inherently broadcasted to all destinations, even when it is not intended. For no extra cost, other receivers will receive packets not addressed to them. In the case where a packet is lost at the receiver, other receivers may receive it successfully. Keeping those packets by receivers for some time enables NC to reduce the number of packets to be transmitted.

NC reduces the number of transmissions by replacing the conventional store-and-forward paradigm in relaying scenarios with a process-and-forward approach. Instead of forwarding packets in the same form as they are received, the intermediate nodes combine the received outgoing packets using an algebraic function such as XOR. All nodes store all the received packets for possible packet decoding purposes. As a result, a typical NC mechanism is composed of two main operations [6, 10]:

- Coding outgoing packets on intermediate nodes.
- Decoding incoming packets upon their reception on nodes.

The main concept of NC is presented through examples and is also sketched in **Figure 2**. Let us consider the situation where destination node D_1 can only hear transmissions from relay node R and source S1. Similarly, destination D_2 can only hear transmissions from source S_2 and relay node R. S1 has a packet p_1 for D_2 and S_2 has a packet p_2 for D_1. S_1 and S_2 send their packets separately to R, using two transmissions. In the first example (i.e., **Figure 2** (without NC)), the relay node R cannot transmit two packets at the same time. Thus, again two transmissions are used to transmit packets p_1 and p_2.

Referring to the **Figure 2** (with NC), it shows the case of the same network but using NC. The relay node R has enough processing power to code two packets, that is, the R node performs a coding operation, for example, linear operation over the p_1 and p_2; thus creating a coded packet of the same size as largest of p1 and p2. Node R can now by sending only one packet forward both p_1 and p_2 to its destination nodes. D_1 can decode the coded packet as it is familiar with the content of p_1 and similarly D_2 can also decode coded packet as it knows the content of p_2. Instead of using four transmissions, the broadcast nature of the media has been embraced and only three transmissions were needed.

The slight overhead that can be seen here is the buffer space requirement as well as additional processing in encoding and decoding the packet. With the advancement in solid states like high speed processors, and high speed and large capacity memories, these overheads are well taken care of. The bandwidth is limited especially in wireless networks. Using NC, we can efficiently utilize the bandwidth of the network.

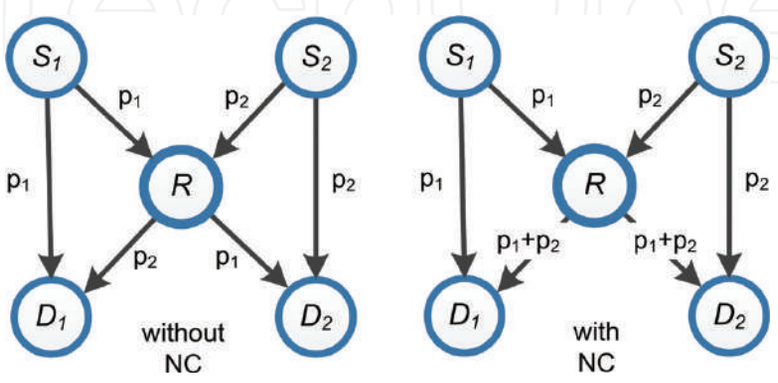

Figure 2. Network coding example.

http://dx.doi.org/10.5772/intechopen.71784

3. Network coding-assisted retransmission scheme

3.1. Concept

Consider the system setup illustrated in **Figure 3**. System is intended for transferring multiple video streams to multiple clients. In depicted example, streaming server is streaming two channels (streams *A* and *B*) to *Client* 1 and *Client* 2, respectively. Packets that are not successfully delivered in the first transmission are retransmitted. Clients signal the server on the not received packets using signalization, for example, in our case with signalization.

Figure 4 shows similar system. The difference is in the retransmission concept. In the first system, every packet that has not been received is retransmitted individually (e.g., five retransmissions). The second system codes multiple packets together and generally uses fewer transmissions (e.g., three).

For the system depicted in **Figure 4**, the design parameters were selected as follows:

- Only packets that require retransmission are transmitted.
- Packets are transmitted as late as possible, that is, after the retransmission timeout (RTO) or opportunistically.

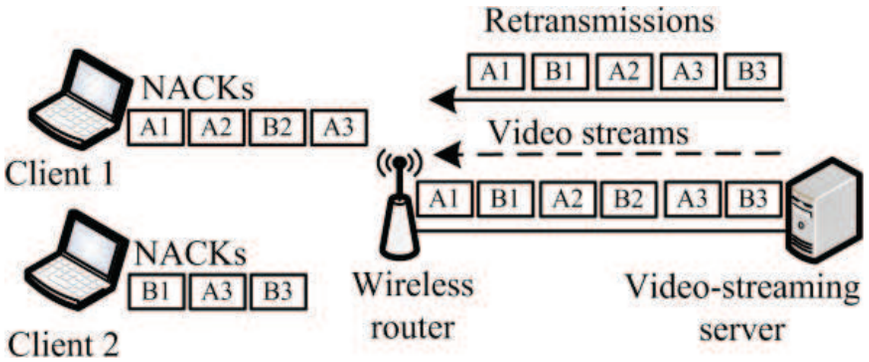

Figure 3. Retransmissions using traditional retransmission scheme.

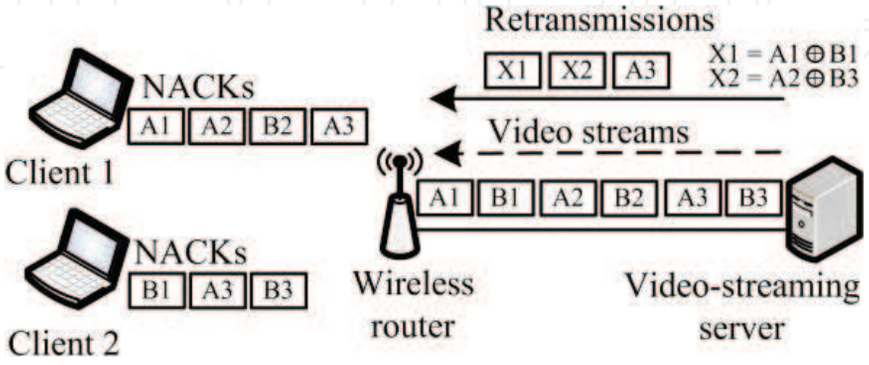

Figure 4. Retransmissions using NC-assisted retransmission scheme.

- All coded packets must be decodable on all the clients.
- Packets not received by any of the clients are sent out as they are, that is, not coded.

The streaming server keeps track of packets received for each of the clients. Information about unsuccessful received packet is provided through the negative acknowledgement (NACK) packet. Current status of the received packets at individual clients is presented in a transition table (e.g., **Table 1(a)**). *M* rows in the table correspond to packets that have not been received by at least one of the clients, and *N* columns correspond to the clients. Packets that have been received by all clients are not presented in the table. Packets with the lowest index have been present in the table for the longest period. There are three different states that indicate packet status:

- *State* 1: packet successfully received by the client.
- *State* 0: packet intended for the corresponding client not received means that packet needs to be retransmitted.
- *State* 2: packet not intended for the corresponding client not received means that packet does not need to be retransmitted. This state is required in the coding procedure as we explained below.

Packet status is represented in the transition table for the time needed to receive feedback from all the clients as explained in next section. Transmission and coding processes are based on the coding table (e.g., **Table 1(b)**) that is obtained from transition table and where only packets that require retransmissions are represented. As soon as packet status is noted in the coding table, the packet can be opportunistically transmitted. In coding table, two states are used to describe the packet status of the clients. Namely, not received packet is indicated by state 0, while packet received on the corresponding client is indicated by state 1. However, in the coding table, we are not presenting the packets that do not need to be retransmitted as they were not transcript from transition to coding table.

NC algorithm for making decisions on which packets to code together is presented in Algorithm 1. The algorithm is called after native packet is broadcasted. First, it checks if the first

(a) Transition table

	C_1	C_2
A_1	0	1
B_1	1	0
A_2	0	1
B_2	2	1
A_3	0	2
B_3	1	0

(b) Coding table

	C_1	C_2
A_1	0	1
B_1	1	0
A_2	0	1
A_3	0	1
B_3	1	0

Table 1. Transition and coding tables.

http://dx.doi.org/10.5772/intechopen.71784

packet has exceeded *RTO*. Second, algorithm inspects the statuses of the first packet on the clients using the coding table (that is first row) and decides if it is codable. Packet is considered codable, if it has been received at least by one of the clients. Otherwise, it is transmitted as is. Last, the algorithm tries to code the packet with as many packets as possible (even the ones that have not reached the *RTO*) but prioritizes packets that have been waiting for a longer period.

Definition 1. Algorithm considers two packets codable, if coded packet can be decoded by all the clients.

In practice, this means that all sums over the corresponding packet columns from the coding table are not less than the number of coded packets $N_{CODED} - 1$. As shown in [5], client can decode coded packet if it has previously received at least $N_{CODED} - 1$ native packets coded in the encoded packet.

Algorithm 1

```
1:  if (P1 exceed RTO)
2:      if (P1 is codable)
3:          k = 1;
4:          coded_packets [k] = &P1;
5:          temp_coding = coding_table [first_row];
6:          coding = temp_coding [];
7:          for (m = 2; m <= M; m++)
8:              codable = 1;
9:              for (n = 1; n <= N; n++)
10:                 temp_coding[n] = temp_coding[n] + coding table [m, n];
11:                 if (temp_coding [n] < k)
12:                     codable = 0;
13:                     temp_coding = coding;
14:                     break;
15:                 end if
16:             end for
17:                 if (codable)
18:                     k++;
19:                     coding = temp_coding;
```

```
20:                 coded_packets [k] = &P_m
21:               end if
22:             if (k == N)
23:               break;
24:             end if
25:         end for
26:     end if
27:     if (k > 1)
28:         encode packets from coded_packets
29:         sent encoded_packet;
30:     else
31:         sent P_1 uncoded;
32:     end if
33:         update coding_table;
34:     end if
```

Example 1: Let us use the example from **Table 1 b** to explain the algorithm in practice. When algorithm is initiated, it first checks if the *RTO* for the first packet A_1 has exceeded. Then, it checks for the packet A_1 if it is codable. Since these conditions are fulfilled, algorithm examines if the second packet B_1 is codable with A_1. Referencing to the *Definition* 1, packets are codable, that is, sum of their corresponding columns is not less than *k*. In this example, only two packets can be coded together, hence the algorithm stops the coding procedure for packet A_1. Packets A_1 and B_1 are coded together and sent out using one transmission. If there were more clients, the algorithm would look for other coding opportunities trying to code more packets together. Further, when *RTO* is reached for packet A_2 algorithm, tries to code it with the next packet in the coding table A_3. Packets do not meet requirement from *Definition* 1, hence algorithm matches A_2 against the next packet, that is, B_3. In this case, packets are codable, thus, sent out in one transmission as together coded packet. Since there are no more packets left to code it to, lastly, packet A_3 is sent out as is. However, in such cases, where there is only one packet left in the coding table, is rarely encountered in practice. Simultaneously with packet transmissions, there are requests for retransmissions for new packets received. Thus, new packets are coming in the coding table to which A_3 would be matched for new coding opportunities.

In a given *Example 1* using proposed approach, five retransmitted packets are transmitted using only three transmissions. Even higher gains can be obtained in cases with more clients.

3.2. Implementation details

This section describes implementation details of the mechanisms required on the server and client.

3.2.1. Client side

On the client, *signalization*, *overhearing,* and *packet decoding* are the main processes and are described in greater detail in the following:

- *Signalization*: *NACK* packets are the only stand-alone packets used for signalization purposes and inform server in which packets have not been received on the clients. Two types of *NACK* packets are foreseen: hard *NACK* and soft *NACK*. Hard *NACK* is a packet sent by the client that has missed a packet from a stream currently in use (i.e., marked with 0 in the transition table). Soft *NACK* is a packet sent by the client that has not received packet for stream that is not intended for it (i.e., marked with 2 in the transition table). Soft *NACKs* only inform the server on the status of the received packets, though the packet not received is not required by the client. *NACK* packets are sent to the server using unicast mechanism, as it is a reliable mechanism and packets are unlikely to get lost.
- *Overhearing*: all clients listen to all the transmissions, even the ones not intended for them and store all packets in the packet pool, for decoding purposes.
- *Decoding*: with every received packet, the client checks if it is native or coded packet. In the case when a coded packet is received, the process checks the packet pool. If enough packets have been received (and stored in the packet pool), the client has enough information and it decodes the coded packet. Using previously stored packets and the *XOR* operation against coded packet, a native packet, previously not received is obtained [6].

3.2.2. Server side

Broadcasting, *NACK handling,* and *coding* processes take place on the server side, namely:

- *Broadcasting*: all packet transmissions from the server to clients are carried out using broadcast.
- *NACK handling*: for every *NACK* packet that server receives updates in transition table are made. Packet status is recorder in transition table only for a short time in order to gather *NACKs* for the packet from all the clients.
- *Coding*: after every broadcast of native packet server searches for coding opportunities in the coding table. If an opportunity is found, first packets are coded together with as many packets as possible sent out in one transmission to all clients. Otherwise, it is not coded than sent out as is.

3.2.3. Overhead estimation

NC-assisted retransmission scheme brings an additional overhead into the network in terms of additional packets and headers. They are depicted in **Figure 5**. All packets have additional

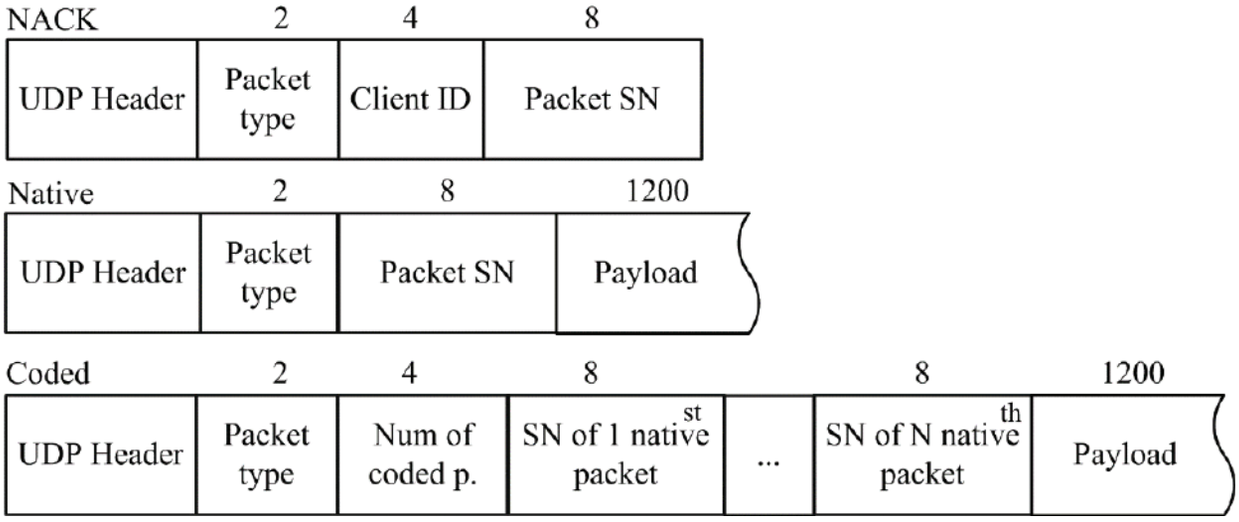

Figure 5. Packet headers.

headers such as *packet type* field indicating that a packet is signalization (*NACK*), native, or coded packet (2 bytes). Native packet has additional *sequence number* (8 bytes) of a packet used for identification. In the case of a coded packet, *sequence number* for each of the encoded packet is given. Also, coded packet carries information on how many packets are coded in the encoded packet (4 bytes). Native packet has *Payload* (1200 bytes) field where video content is placed. Coded packet payload is the same as the native packet and it is composed of *XOR-ed* payloads of every encoded native packet.

Signalization (*NACK*) packet contains the network coding unique information such as: *Client ID* (4 bytes) field, which identifies the sender of the client.

4. Practical evaluation

4.1. Wi-Fi test bed

In order to evaluate the proposed scheme, we deployed IEEE 802.11 network test bed consisted of streaming server, access point, and multiple Wi-Fi clients. Server and clients were laptops with different hardware, for example, different wireless interfaces. For the access point, we used wireless router Linksys WRT54GL. Server was connected to the wireless router via Ethernet interface while clients were connected via WLAN interface. In order to perform tests, we used a third party firmware (i.e., DD-WRT) in our wireless router, because the original firmware was not capable of transmitting a multicast channel through it. Wireless router configuration was fixed during the experiments. Packets size was constant (i.e., 1210 bytes). Inter-arrival time between packets was also constant (i.e., 6 ms), resembling video-streaming application. Results were presented for the shortest time intervals to observe steady state conditions. Two client setups, mobile and static were used for the evaluation and are presented in the next sections.

4.1.1. Mobile client setup

In this scenario, experiment was set up with server and six clients, where each client position has changed once, during the experiment.

Server streamed one UDP 608 MB stream. If it streamed one packet every 6 ms (inter-arrival time between packets) that would be approx. 166 packets per second. The size of a single packet is 1200 bytes. Thus, the data rate was 1.525 Mbps.

The experiment started with all clients placed in the room with the router. Every 7 min, one client at a time was relocated to the nearby room. By moving clients to the nearby room, we wanted to observe how delivery probabilities were changing during the time. We assumed that delivery probabilities would decrease, due to wall obstacles between the server and the clients. Further, obstacles had caused packet loss, which we supposed would affect delivery probability of single clients in the nearby room.

Next, with decreased delivery probabilities, we expect more coding opportunities and higher bandwidth reduction, which we will discuss later in the result section.

4.1.2. Static client setup

In the second scenario, where clients were static and located in one room, four experiments were carried out, each with different number of clients (4, 6, 8, and 10). Server streamed one UDP stream in total of 122 MB and 1.525 Mbps data rate. Value of data rate is calculated as in for mobile client setup. Using this architecture setup, we wanted to observe if the number of clients will affect improvements in the bandwidth.

We expect to reduce more of the bandwidth, because with more clients we assume more coding opportunities, which means fewer transmissions and therefore better bandwidth reductions.

4.2. Evaluation metrics

Several performance metrics were used to evaluate the performance of the proposed scheme. All the presented results were observed over the sample period T_S (i.e., 20 s).

N_N is the number of native packets sent. N_R notes the number of retransmitted native packets. N_{RNC} is the number of transmissions performed to retransmit N_R packets, where $N_R \geq N_{RNC}$ if network coding is used. N_{Di} presents number of successfully received packets at i-th client, while N_C presents the number of clients.

Bandwidth reduction B_R is calculated as the proportion of difference of the N_R and N_{RNC} packets to the sum of N_N and N_R packets. We use B_R to show the share of bandwidth we reduced by using proposed approach.

$$B_R = \frac{N_R - N_{RNC}}{N_N + N_R} \cdot 100\% \tag{1}$$

Client delivery probability DP_i is defined for individual clients as:

$$DP_i = \frac{N_{D_i}}{N_{N_i}} \cdot 100\% \tag{2}$$

Delivery probability *DP* is an average of client delivery probabilities:

$$DP = \frac{1}{N_C} \sum_{i=1}^{N_C} DP_i \tag{3}$$

Client gain G_i is defined for *i*th client as:

$$G_i = 1 - \frac{N_{Ri}}{N_{RNC_i}} \cdot 100\% \tag{4}$$

Gain *G* is average client gains:

$$\mathrm{G} = \frac{1}{N_C} \sum_{i=1}^{N_C} G_i \tag{5}$$

Coding table size (CTS) refers to the number of packet-statuses on the clients noted in the table (note that only packet that requires retransmission is present there). Size is sampled periodically, after broadcasting native packet.

C_{AVG} is the average number of native packets sent in one retransmission (average number of encoded packets).

4.3. Experimental results

Results are presented individually for two client's setups that we explained above, that is, mobile and static. Mobile client's results give more detail results of described performance metrics above, while static client's results just discuss the number of clients depended of the gain.

4.3.1. Mobile client results

Bandwidth reduction B_R of proposed approach is presented in **Figure 6**. Straight lines in the figure indicate transition periods at which clients were relocated and divide figure in equal rectangles. For example, in the second rectangle from the left, five clients were located in the router room and one was in the room nearby. From this figure, we can observe that B_R increases over the time. The results show that in the given testbed, we have been able to save 6% of total consumed bandwidth per average. The value in observed time interval ranged between 4 and 8%.

DP is shown in **Figure 7** and we can see that it is over time lowering. This is expected because we were moving clients away from the router over the time.

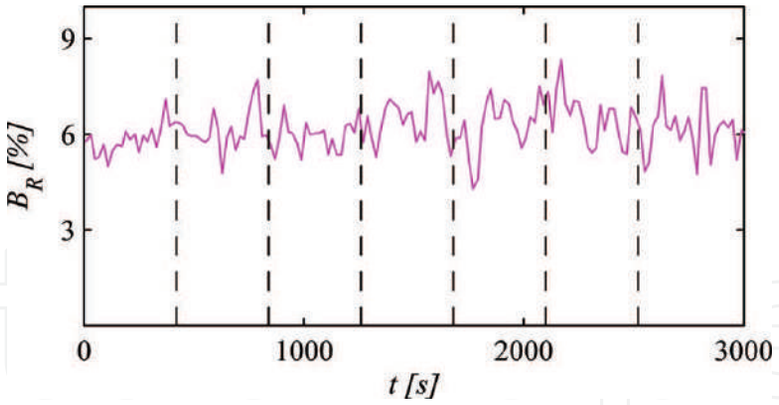

Figure 6. Bandwidth reduction B_R [%] in dependency of time t [s].

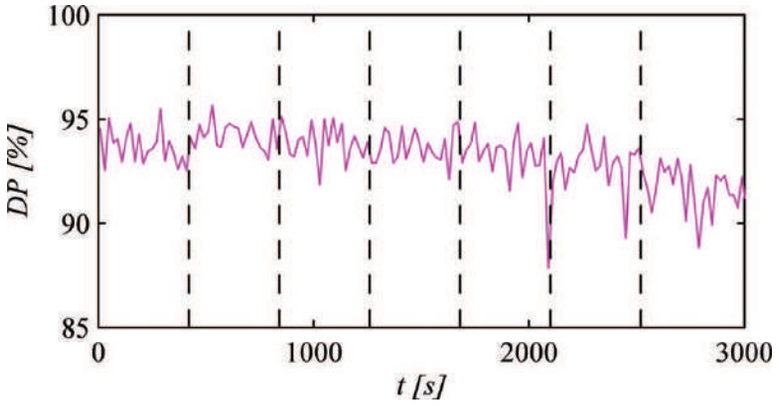

Figure 7. Delivery probability *DP* [%] in dependency of time *t* [s].

In the following, we show relations between average numbers of coded packets C_{AVG}, the number of transmissions performed to retransmit N_R packets, and gain *G* depicted in **Figure 8**. If C_{AVG} falls, N_{RNC} increases, and *G* decreases. For example, let us examine graphs in the time interval between 2100 and 2180s where very apparent case of described situation is shown. If more native packets are coded together, fewer packets need to be transmitted, thus *G* is increased. For example, for t = 2111 s, C_{AVG} = 1.831, N_{RNC} = 350, and G = 45%. Contrarily for t = 2130 s, C_{AVG} = 1.23, N_{RNC} = 1278, and G = 19%.

In the next step, we investigate *DP* versus the *G* as depicted in **Figure 9**. *DP* values range from 80 to 96%, while the corresponding values for *G* are from 18 to 46%. The majority of points from graph are located in the area with high *DP* and high *G*. There are several points that are far away from the cluster.

4.3.2. Static clients results

We investigate how the proposed scheme performs with different number of clients (i.e., 4, 6, 8, and 10). Results are shown in **Figure 10** for B_R. Observed interval is between 0th and 250th. Results show that highest B_R values are observed when the number of clients is the highest

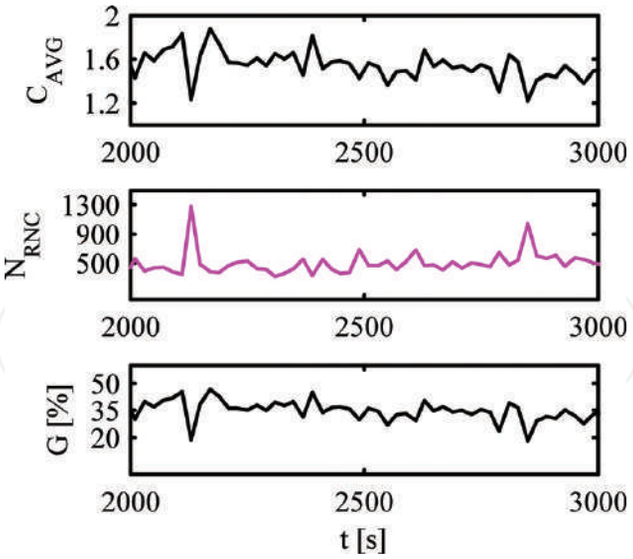

Figure 8. Average number of coded packets CAVG, coding table size CTS, and gain *G* [%] over time.

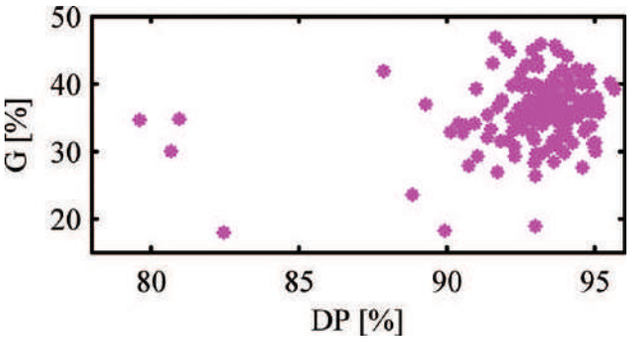

Figure 9. Gain in *G* [%] dependency of delivery probability *DP* [%].

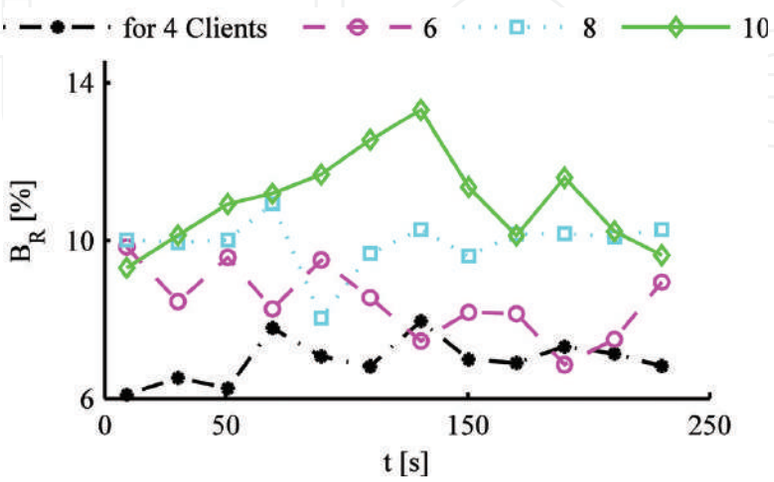

Figure 10. Bandwidth reduction B_R [%] over time for different number of clients.

(e.g., average B_R values for 4, 6, 8 and 10 clients are: 7, 9, 10, and 13%, respectively). When the number of clients increases, B_R improves at the same time, that is, when the number of clients is higher, there are more packets that get lost, hence there are more entries in the coding table CTS and coding algorithm is able to find more coding opportunities.

5. Conclusion

In this chapter, the approach for improving bandwidth in the last mile wireless broadcast network using network coding was investigated theoretically and practically. We have evaluated the performance of our approach for video-streaming services, such as IPTV, by designing and implementing a specific system solution, for a lossy wireless scenario. Our proposed schemes combine different lost packets from different clients in such a way that all clients are able to recover their lost packets with one transmission by the server. In particular, network coding is used to code and decode packets, as the new way of transmitting packets through the network. Instead of just store-and-forward technique, the server is now able to code packets in a more clever way, and transmit them over the broadcast network.

The implementation of such architecture, in a real scenario, was shown to be feasible. We tested the proposed approach with two different scenarios. It was found that the proposed approach in both cases decreases the number of transmitted packets. As compared to traditional unicast retransmission approach, where every packet is retransmitted separately, the reduction in bandwidth using the proposed network coding assisted retransmission scheme was up to 15%. This is a significant result and the developed scheme should be of great interest to be implemented in throughput demanding systems. In addition, results show that proposed approach saves bandwidth in various situations where users have different terminal equipment and different link quality. We observed the highest gains with high number of clients (i.e., 10 clients), which is also the case in the envisioned application where even higher number of different concurrent streams is anticipated.

Author details

Aleš Švigelj* and Melisa Junuzović

*Address all correspondence to: ales.svigelj@ijs.si

Jožef Stefan Institute, Ljubljana, Slovenia

References

[1] Junuzović M, Alič K, Švigelj A. Wireless broadcast transmission scheme for reliable video-streaming service. WSEAS Transactions on Communications. 2015;**14**:256-266

[2] Ahlswede R, Cai N, Li S-YR, Yeung RW. Network information flow. IEEE Trans. on Information Theory. 2000;**46**(4):1204-1216. DOI: 10.1109/18.850663

[3] Ferreira D, Costa RA, Barros J. Real-time network coding for live streaming in hyperdense WiFi spaces. IEEE Selected Areas in Communications. 2014;**32**(4):773-781. DOI: 10.1109/JSAC.2014.140409

[4] Seferoglu H, Markopoulou A. Video-aware opportunistic network coding over wireless networks. IEEE Journal on Selected Areas In Communications. 2009;**27**(5):713-728. DOI: 10.1109/JSAC.2009.090612

[5] Katti S, Rahul H, Hu W, Katabi D, Médard M, Crowcroft J. XORs in the air: Practical wireless network coding. IEEE/ACM Transactions on Networking. 2008;**16**(3):497-510. DOI: 10.1109/TNET.2008.923722

[6] Alič K, Pertovt E, Švigelj A. Bearing-opportunistic network coding. International Journal of Computers, Communications & Control. 2015;**10**(2):154-164. DOI: 10.15837/ijccc.2015.2.457

[7] Nguyen D, Tran T, Nguyen T, Bose B. Wireless broadcast using network coding. IEEE Transactions on Vehicular Technology. 2009;**58**(2):914-925. DOI: 10.1109/TVT.2008.927729

[8] Xiao X, Lu-Ming Y, Wei-Ping W, Shuai Z. A wireless broadcasting retransmission approach based on network coding. In: ICCSC 2008. 4th IEEE International Conference on Circuits and Systems for Communications; 26–28-05-2008. Shanghai, China. Shanghai: IEEE; 2008. pp. 782-786. DOI: 10.1109/ICCSC.2008.171

[9] Fang W, Liu F, Liu Z, Shu L, Nishio S. Reliable broadcast transmission in wireless networks based on network coding. In: IEEE Conference on Computer Communications Workshops (INFOCOM WKSHPS); 10–15-04-2011; Shanghai, China. Shanghai, China: IEEE; 2011. pp. 555-559. DOI: 10.1109/INFCOMW.2011.5928875

[10] Alič K, Švigelj A. Self-adaptive practical opportunistic network-coding procedure for static wireless mesh networks. Ad-hoc & Sensor Wireless Networks. 2017;**36**(1–4):87-105

Chapter 9

Atmospheric Attenuation of the Terahertz Wireless Networks

Milda Tamosiunaite, Stasys Tamosiunas, Mindaugas Zilinskas and Gintaras Valusis

Additional information is available at the end of the chapter

http://dx.doi.org/10.5772/intechopen.72205

Abstract

The increase of data traffic, a demand for high-speed reliable mobile networks and congested frequency bands raised both technological and regulatory challenges. Therefore, the fifth-generation mobile network (5G) is being developed. Recently, researchers have focused on a very promising terahertz (THz) band (frequencies from 100 GHz to 30 THz), which will allow fast transmission of huge amounts of data. However, transmission distance is limited due to atmospheric attenuation, as THz waves undergo significant absorption by water vapor and oxygen molecules in the atmosphere. Moreover, THz waves are very vulnerable by precipitation. Furthermore, the path of the propagating waves changes due to variations of the atmospheric refractive index. Nevertheless, the THz networks could be perfect candidates for fiber-to-THz bridges in difficult-to-access areas. The aim of this chapter is to present the possibilities and challenges of the THz networks from a point of view of atmospheric attenuation. The results show that simulations of the atmospheric attenuation using real-time data are a powerful tool that should complement technological basis, as it will help to foresee possible failures, extend transmission distance and improve reliability of the THz and other high-frequency broadband wireless networks.

Keywords: broadband wireless communications, terahertz wireless networks, atmospheric attenuation, rain attenuation, refractive index

1. Introduction

Data traffic in wireless communications has been increasing rapidly over recent decades. Edholm's law (resembling the well-known Moore's law for transistors) states that wireless data rates have doubled every 18 months over the last three decades and are quickly

approaching the capacity of wired communication systems [1]. Furthermore, the Internet traffic is expected to reach over 130 exabytes per month by 2018 [2]. The speed limits are based on the Shannon theorem [3], which states that, for a given average signal power, the channel bandwidth limits the maximum data rate that can be attained with a sufficiently low error rate.

The most desirable spectrum to satisfy the wireless needs is the frequency band of 1–10 GHz, whereas propagation losses due to atmospheric absorption and precipitation play a secondary role, and in many cases may generally be neglected[1] [4]. However, the band up to 10 GHz is highly congested. Despite the efforts to improve its efficiency, it is difficult to locate a sufficient amount of free bandwidth. Since current networks are no longer able to cope with the forthcoming load (i.e., Internet of Things (IoT), self-driving cars and so on), recent research has focused on the THz technology, which has a lot of potential owing to a large bandwidth capability, highly directive beams, obtained with relatively small antennas, and, consequently, low transmitter power requirement. Although transmission distance will be limited due to severe effects in the atmosphere, the THz networks are perfect candidates for short-distance communications, such as fiber-to-THz bridges in difficult-to-access areas.

The aim of this chapter is to present the possibilities and challenges of the THz networks from a point of view of atmospheric attenuation. The chapter consists of three parts. The first part is dedicated to the review of the possible applications and basic concepts of the THz wireless networks. In the second part, the main mechanisms of the atmospheric attenuation are presented. This part also includes a brief overview of the basic principles of radio system design and recommendations of the International Telecommunication Union (ITU-R). The third part is based on real-time measurements and simulations using meteorological data.

2. Terahertz wireless networks

2.1. The terahertz band

The terahertz (THz) band (also often called the T-rays or „terahertz gap") consists of electromagnetic waves in the frequency region of 100 GHz–30 THz.[2] One terahertz (1 THz = 10^{12} Hz) corresponds to a vacuum wavelength of 0.3 mm. As terahertz radiation begins at a wavelength of 1 mm and proceeds into shorter wavelengths, it is sometimes called the submillimeter band. The THz band is also called the "terahertz gap," as it divides the microwaves and infrared waves or, in other words, the electronics and optics (**Figure 1**). Both electronics and optics contributed to the development of the THz technology, as photonics has led the way to the realization of many important THz devices, such as the development of the quantum cascade laser (QCL), while electronics contributed with solid-state electronic devices, such as resonant tunneling diodes (RTD) [5].

[1]However, the application cannot be so straightforward. In order to ensure a reliable connection, the attenuation of the atmosphere should be evaluated starting from 1 GHz or even lower frequency.

[2]100 GHz corresponds to 0.1 THz. Perspectives for telecommunications are expected in the region up to 10 THz.

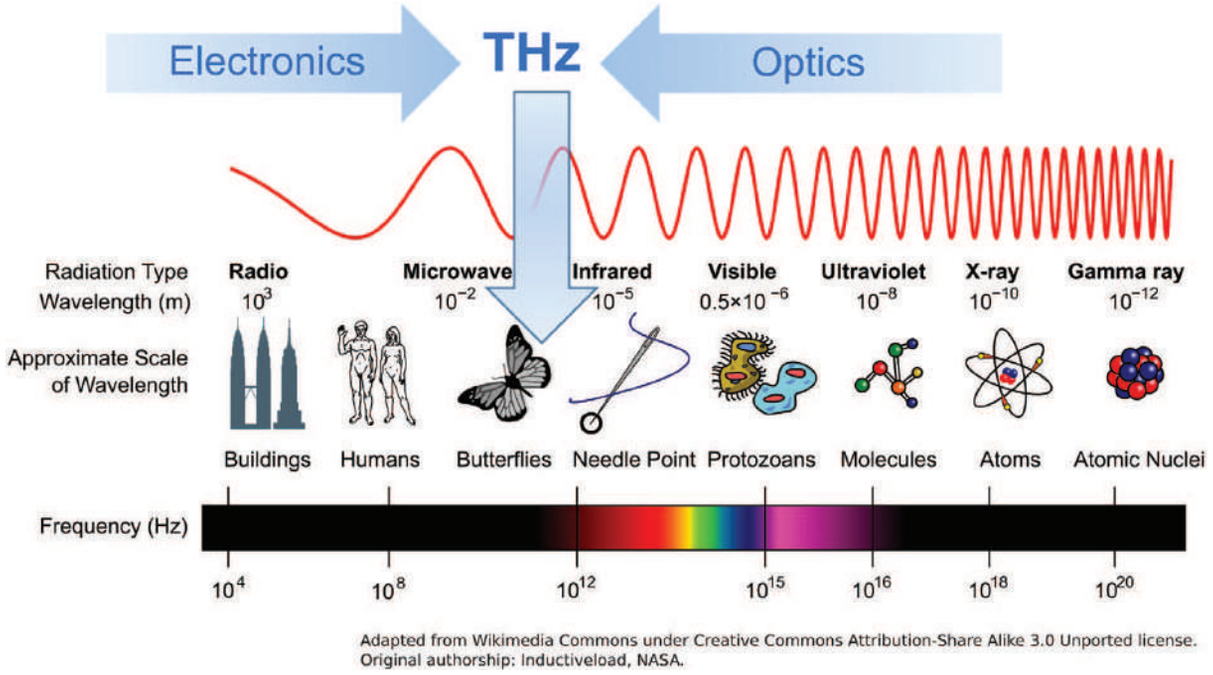

Figure 1. The terahertz (THz) gap. Both electronics and photonics contributed to the development of the THz technology.

The THz band, combined with recent technological innovations, offers wide application possibilities from nondestructive medical imaging, quality control, security issues (i.e., detection of weapons, explosives and narcotic substances, as every material has a distinct signature in its THz spectra [6]), communications and many more. The communication sector can benefit from THz technology in many ways, starting from wireless communications and high-speed data processing, to satellite communications.

2.2. The concept of ultrabroadband THz wireless networks

According to [7], there are several reasons that motivate the use of the THz band for ultrabroadband communication networks. First of all, wireless technologies below 0.1 THz (100 GHz) are not able to support terabit per second (Tbps) links, as available bandwidth limits the achievable data rates (however, compact wireless technologies above 10 THz are not able to support Tbps links). Furthermore, the THz band offers a much larger bandwidth, which ranges from tens of GHz up to several THz, depending on the transmission distance, and it opens the door for the variety of applications that demand ultrahigh data rates. In 2012, a group of researchers have smashed the record for wireless data transmission in the terahertz band. The data rate was 20 times higher than the best commonly used Wi-Fi standard [8]. However, due to technological limitations, the best performance of the THz wireless network is shown under indoor conditions. One of the main challenges is a very high path loss at THz band frequencies, which limits the communication distances[3] [7]. The appropriate frequency band should be determined by the application [9], as the higher the operational frequency,

[3]In addition to all the challenges, the THz Band is not yet regulated. However, the beginning development is accompanied by standardization activities addressing the lower THz range. According to the proposal of the IEEE 802.15.3 group, the frequency range 252–325 GHz is defined as the Thz PHY, and the links using Thz PHY are called THz links.

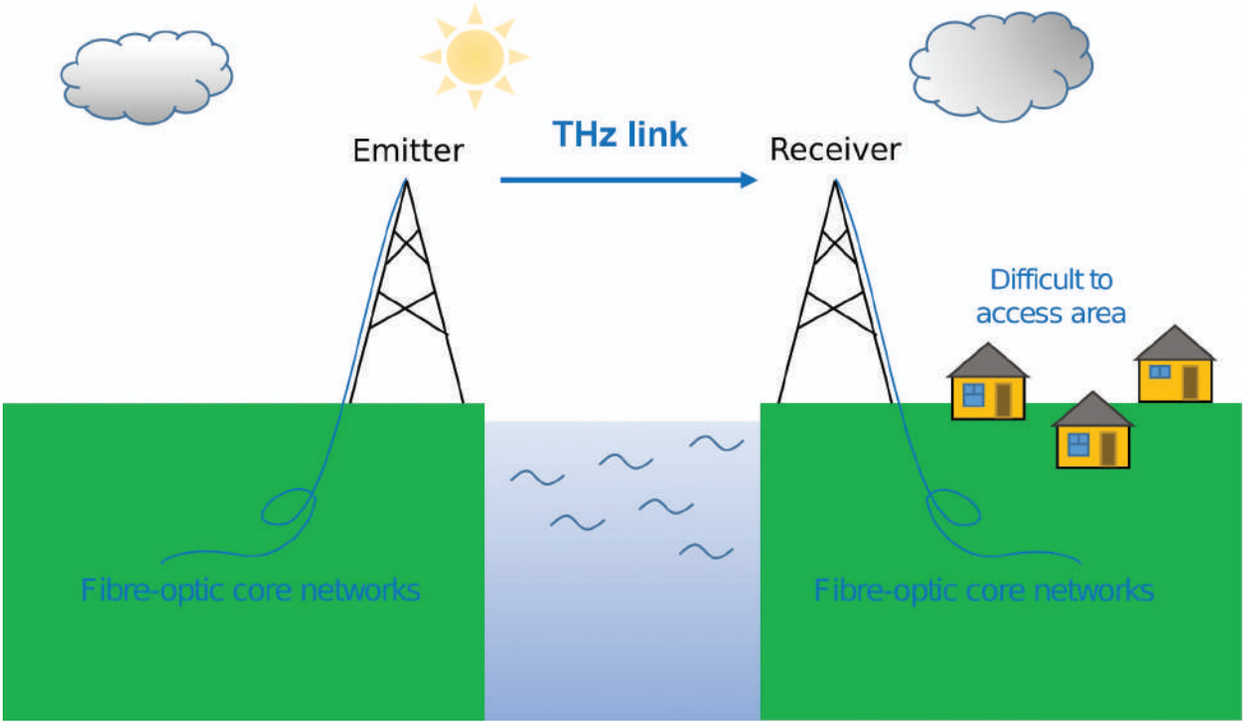

Figure 2. The concept of fiber-to-THz radio bridges for connection between a fiber-optic link and a THz link.

the shorter the distance (~100–150 GHz for long distance (~1–10 km), <350 GHz for medium distance (~100 m–1 km) and <500 GHz for indoor (~10–100 m) communications) which THz wave can travel without crucial distortions. Bearing in mind the distance problem, THz communications could benefit from the well-developed fiber-optic links. The wireless-over-fiber technology was introduced in [10]. In fact, owing to low losses in the optical fiber cables for long-haul transmission, wireless-over-fiber is a very promising technology for the difficult-to-access areas (**Figure 2**). In addition, the basic principles of the 5G technology can be adapted, such as the massive Multiple Input, Multiple Output (MIMO) antennas integrated into base stations [11] and densely deployed small cells [12] that are able to maintain a decent level of signal quality in areas with high density of mobile users [13]. Other solutions are also possible. For example, in [14], a concept of mirror-assisted wireless coverage system is suggested. The smart antennas are utilized with a number of moveable dielectric mirrors that act as reflectors for the THz waves, creating a virtual line of sight.

However, as was concluded in [15], the transmission capacity of a system with a given transmission power depends critically on channel properties like path losses, antenna misalignment and interference due to reflection and scattering.

3. Propagation modeling (atmospheric attenuation)

The design techniques of the new telecommunication links take into account a series of various factors that are comprehensively explained by Freeman [4] and regulated by the International Telecommunication Union (ITU-R). If a beam would propagate in free space

without atmosphere, the path would be a straight line. However, the atmosphere is always present. In this chapter, the atmospheric effects on propagation are briefly overviewed in terms of the THz communications. A more detailed description of the atmospheric effects is provided in [16].

3.1. Free-space loss vs. actual atmosphere

A free-space path loss (FSPL) is inevitable attenuation in the line-of-sight path through free space. In general case, the free-space loss rises with the square of the carrier frequency and link distance (i.e., 100 dB for a 10-m THz link at a carrier frequency of 300 GHz [17]). In actual atmosphere, there are additional sources of atmospheric loss that affects the amplitude, phase and polarization of electromagnetic waves. Generally, these effects could be predicted. The prediction procedures consist of few steps, and the meteorological data (rain rate, temperature, humidity, etc.) are required.

3.2. Gaseous absorption

Due to the presence of gas and water molecules in the atmosphere, electromagnetic wave travels more slowly, and part of its energy is scattered or absorbed. Some molecules present in a standard atmosphere are excited by the specific frequencies in the THz band. An excited molecule internally vibrates, and as a result of this vibration, part of the energy of the propagating wave is converted into kinetic energy and is simply lost. The necessary parameters to characterize the different resonances for different molecules are collected, contrasted with real measurements, and compiled into HITRAN database [18]. Considering the standard atmospheric composition (mostly molecular oxygen and nitrogen), the gaseous attenuation, γ_g (in dB/km), up to 0.350 THz (accurate model) and 1 THz (general model) can be evaluated using procedure described in [19]. For distances below 1 m, molecular absorption loss is considered to be almost negligible. When transmission distance exceeds 1 m, molecular resonances become significant.

3.2.1. Water vapor

More than any other region of the electromagnetic spectrum THz region is very vulnerable by water molecules. Being a polar molecule with a nonlinear molecular orientation, water displays a strong absorption line for nearly all of its rotational modes [20]. Therefore, it is worth to mention water vapor, which, being minor constituent of the atmosphere, together with oxygen, is the main contributor to gaseous attenuation. Hence, the gaseous attenuation, γ_g, is a sum of attenuation due to water vapor and oxygen, and the path loss due to atmospheric absorption is estimated as multiplication of gaseous attenuation and path length, d,

$$A_G = \gamma_g d. \tag{1}$$

In the molecular absorption spectrum, there are several regions of relative transparency between the absorption peaks. Those regions are called transmission windows. Under standard atmospheric conditions, transmission windows are present at about <0.300, 0.330–0.370, 0.390–0.440, 0.625–0.725, and 0.780–0.910 THz (**Figure 3**). When the frequency exceeds 1 THz, the radio wave undergoes significant absorption by water vapor and oxygen molecules in the

atmosphere [9]. In [21], an accurate terahertz time-domain spectroscopy (THz-TDS) characterization of water vapor from 0.2 to 2 THz was reported. The results agreed with the previously predicted and measured attenuations for the weak water lines, but showed more attenuation for the relatively transparent windows between these lines.

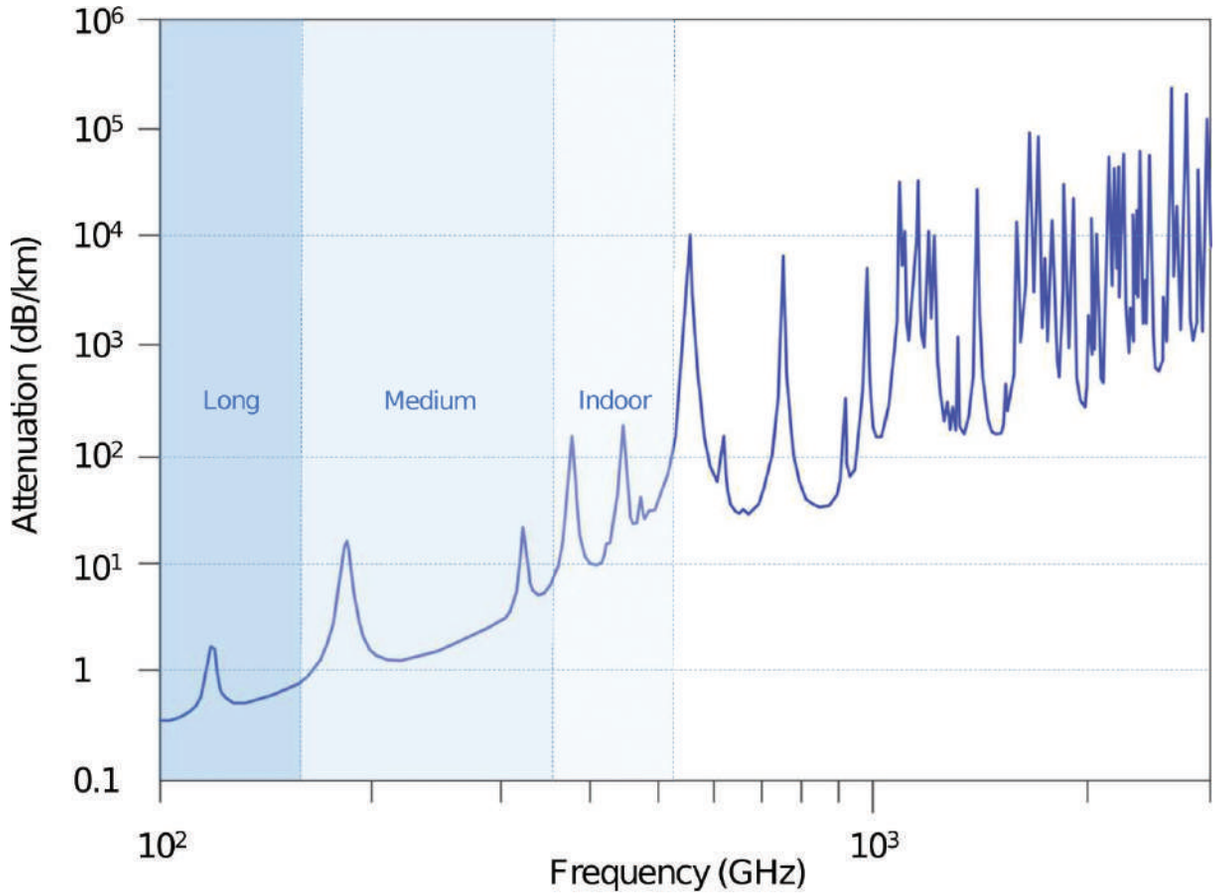

Figure 3. Transmission distance in the THz band is limited by the atmospheric attenuation. Water vapor absorption spectra indicate several transmission windows (the regions of relative transparency between the resonance peaks); when the frequency exceeds 1 THz, the radio wave undergoes significant absorption.

3.3. Precipitation

3.3.1. Rainfall

The effect due to hydrometeors, especially rain, is the most severe. The main mechanisms of the attenuation due to rainfall are absorption and scattering. When an incident electromagnetic wave passes over an object that has dielectric properties different from the surrounding medium, some energy is absorbed (this energy heats the absorbing material) and some is scattered (the smaller the scatterer, the more isotropic it is in direction with respect to the wavelength of the incident energy) [4]. It is a common practice to express the excess attenuation due to rainfall as a function of precipitation rate, which depends on liquid water content and the fall velocity of the raindrops, which in turn depends on drop size distribution (DSD). There are various raindrop size distributions; the most popular is the Laws and Parsons distribution. However, dealing with raindrop size distribution is a complex task, because the

shapes of actual raindrops are far from the usually depicted spherical or tear-drop shapes, as larger drops become flattened and eventually break into smaller droplets [22].

One of the most accepted methods of dealing with excess path attenuation due to rainfall is an empirical procedure based on the approximate relation between excess path attenuation A (in dB) and the rain rate R (in mm/h) [23]:

$$A_{dB} = a R^b, \tag{2}$$

where a and b are functions of frequency. Horizontally polarized waves suffer greater attenuation than vertically polarized waves, so there are different a and b values for vertical and horizontal polarization. The values of a and b can be found in [23].

For frequencies above 100 GHz, the attenuation is considered to be about 10 dB/km in the case of heavy-rain conditions (R = 25 mm/h). However, empirical methods must be applied with caution. Most often, the rain rate of the rainfall is calculated using averaged hourly, daily or even annual data. For path design above 10 GHz, where the path availability better than 99.9% is required, such averaged statistics are not sufficient, as several weeks of light drizzle will affect the overall long-term path availability much less than several good short-lived downpours [4]. In fact, such downpours are cellular in nature and appear in so-called rain cells. To trace such downpours, "one-minute" rain rate values, $R_{(1\,\mathrm{min})}$ (in mm/h), are required. Since data with such accuracy are rarely collected, the "one-minute" rain rate values (integration time is 1 min) can be estimated from various models [16]. However, those models are also based on averaged data; therefore, in territories of varying climate conditions, it is suggested to specify the conversion formula in accordance with the peculiarities of the climate. As the practice shown, the actual "one-minute" rain rate values tend to be higher than the ITU-R suggested values, and it is the main reason for the unexpected telecommunication failures during downpours.

3.3.2. Other precipitation

There are other meteorological phenomena. In example, hail causes only a small attenuation due to rain. The effect of snow depends on temperature, flake size, and water content. Fog and clouds can be treated as very light rains (small droplets or/and ice crystals). In this chapter, other precipitation sources will not be discussed. More information can be found in [4, 16].

3.4. Variations of the atmospheric refractive index

In the atmosphere, the propagating radio beam encounters variations of the atmospheric refractive index. Due to these variations, the ray-path becomes curved, and the fading occurs. The radio refractive index is defined as the ratio of the velocity of propagation of a radio wave in free space to the velocity in a specified medium. At standard atmosphere conditions near the Earth's surface, the radio refractive index has a value of approximately 1.0003. The atmospheric refractive index, n, can be calculated by the following formula:

$$n = 1 + N \times 10^{-6}, \tag{3}$$

where N is the atmospheric refractivity.

According to the procedure described in [4], the atmospheric refractivity is expressed by:

$$N = \frac{77.6}{T}\left(P + 4810\,\frac{e}{T}\right), \tag{4}$$

where P is atmospheric pressure (in hPa), e is water vapor pressure (in hPa) and T is absolute temperature (in K). This expression may be used for all radio frequencies (with the error less than 0.5% for frequencies up to 100 GHz).

The water vapor pressure is given by

$$e = \frac{H e_s}{100}, \tag{5}$$

$$e_s = a \exp\left(\frac{bt}{t + c}\right), \tag{6}$$

where H is relative humidity (in %), t is temperature (in °C), e_s is saturation vapor pressure (in hPa) at the temperature t (in °C), and the coefficients a, b, c are a = 6.1121, b = 17.502, c = 240.97 (for water, valid between −20°C and +50°C, with an accuracy of ±0.20%) and a = 6.1115, b = 22.452, c = 272.55 (for ice, valid between −50°C and 0°C, with an accuracy of ±0.20%).

4. Simulations using real-time data

The main challenge of the radio system design is the reliable source of data. When dealing with atmospheric attenuation, it is very important to gather as reliable as possible metrological data. Unfortunately, data of such accuracy are rarely available. In this part, simulations based on real-time data are presented.

4.1. Rain rate integration time problem

As mentioned above, the mostly available meteorological data are not sufficient for the radio system design, as averaged meteorological data suppress the peak values of significant events, such as downpours. Therefore, 1-min integration time should be used if available.

In **Figure 4**, the data of the heavy-rain event are presented. During 6-h lapse, the rain intensity differed from light to heavy rain, and 37 mm of rain was accumulated until midnight (marked as Precip. Accum.). At the same time, the rain intensity was measured (R-value (10 min)). For technical reasons, the measurements were carried out in 10-min intervals. In addition, 1-min rain rate value, $R_{(1\,\mathrm{min})}$, was calculated, using the Moupfouma and Martin method [24]:

$$R_{(1\,\mathrm{min})} = \left(R_{(\tau_{\mathrm{min}})}\right)^{0.987\tau^{0.061}}, \tag{7}$$

where $R_{(\tau_{\mathrm{min}})}$ is the rain rate value (in mm/h) measured in lapse of time τ (in minutes).

http://dx.doi.org/10.5772/intechopen.72205

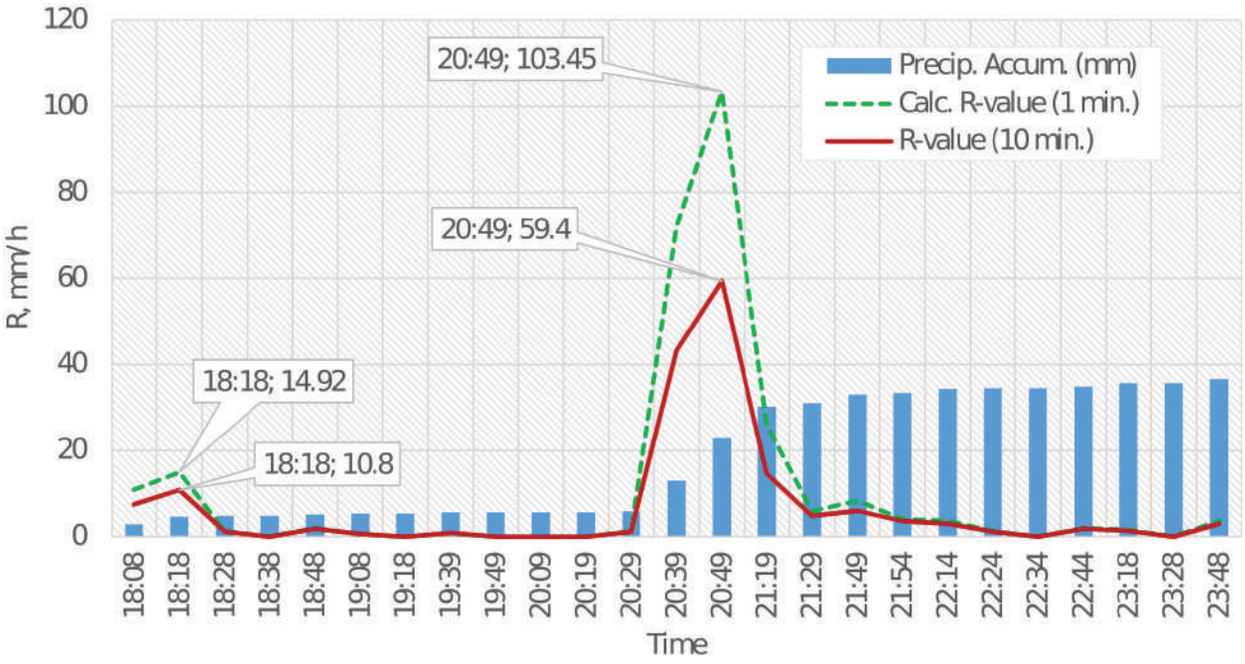

Figure 4. Heavy-rain event. The peak values of the rain rate at the different aggregation times are presented. According to measurements, the maximum *R*-value was *R* = 59.4 mm/h at 20:49; the maximum calculated 1-min *R*-value was almost double, *R* (1 min)=103.45 mm/h. Both of these values are higher than the ITU-R suggested value *R* = 35 mm/h.

According to measurements, the maximum *R*-value was *R* = 59.4 mm/h at 20:49. However, calculated 1-min *R*-value was almost double, $R_{(1\text{min})}$ = 103.45 mm/h. Both of these values are higher than the ITU-R suggested value *R* = 35 mm/h [25].

In **Figure 5**, calculated values of rain attenuation at 0.1 THz (or 100 GHz; the minima of the THz range) electromagnetic waves are presented. As can be seen, the results are different for 1- and 10-min integration times. One-minute rain rate value reveals the peak attenuation being 32.27 dB/km for horizontally polarized electromagnetic waves and 31.55 dB/km for vertically polarized ones. The values calculated using 10-min integration time are lower (22.11 and 21.02 dB/km, respectively). However, when the rain rate starts to fall, the integration time and polarization become less important, as the results in all cases are nearly similar.

In **Figure 6**, the same rain event is presented. The difference is that the *R*-values were calculated using more widely accessible averaged rainfall data with integration time of 1 h and 6 h (standard). In these cases, the downpours are suppressed and delayed (*R* = 24.6 mm/h at 21:19 according to hourly data; *R* = 6.56 mm/h at 23:18 according to 6-h average data).

As can be seen in **Figure 7**, the impact of the suppressed and delayed *R*-values on the attenuation of the propagating 0.1 THz electromagnetic waves is significant and the results are distorted in comparison with the **Figure 5**. The low attenuation values become higher, and the peak values are lower (12.13 dB/km for horizontally polarized waves in comparison with 32.27 dB/km in **Figure 5**). The 6-h (standard) *R*-values (see inset in **Figure 7**) determine very low and delayed attenuation values.

The same calculations were performed for electromagnetic waves with operating frequency of 0.3 THz (or 300 GHz; in many cases, this frequency is considered as a realistic candidate

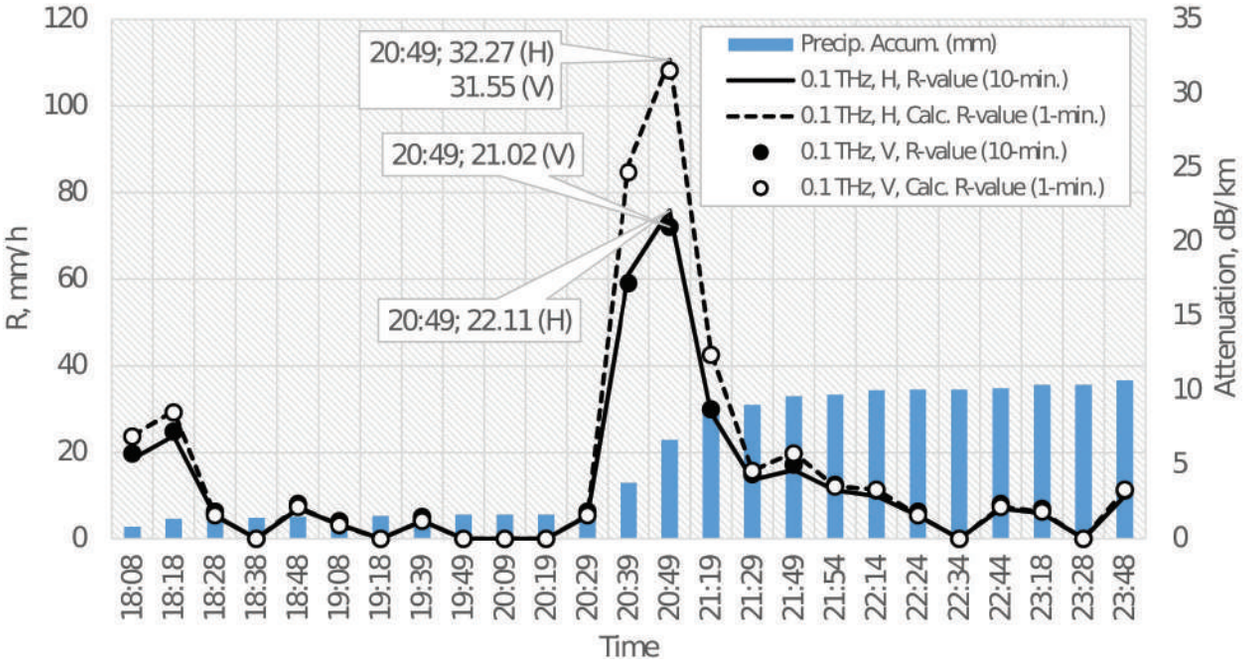

Figure 5. The calculated values of rain attenuation at 0.1 THz using real-time *R*-values. The results differ with integration time. One-minute rain rate value reveals the peak attenuation being 32.27 dB/km for horizontally polarized electromagnetic waves and 31.55 dB/km for vertically polarized ones when the rain rate is 103.45 mm/h.

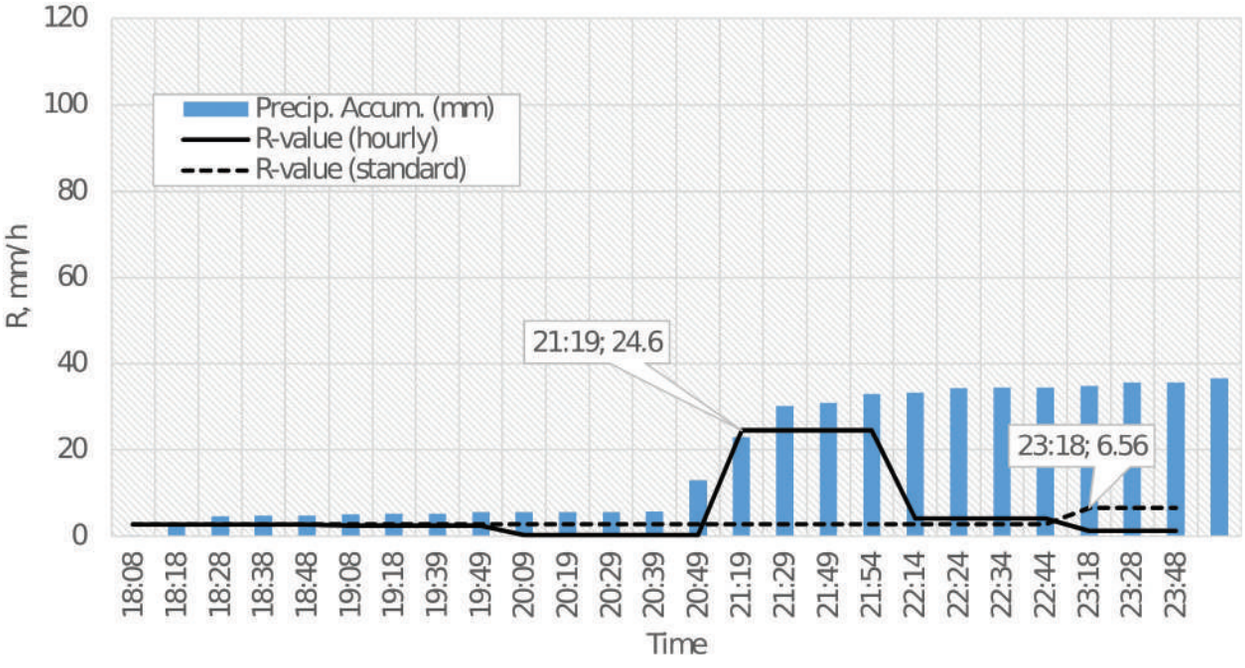

Figure 6. The *R*-values calculated using averaged hourly meteorological data. The downpours are suppressed and delayed in comparison with **Figure 4**.

for the THz communications). The results are presented in **Figure 8**. As can be seen, the tendencies are the same as for 0.1 THz. However, for 0.3 THz, the calculated attenuation values are smaller than for 0.1 THz (according to model, for frequencies higher than 0.1 THz, the rain attenuation slightly decreases) (**Figure 9**).

http://dx.doi.org/10.5772/intechopen.72205

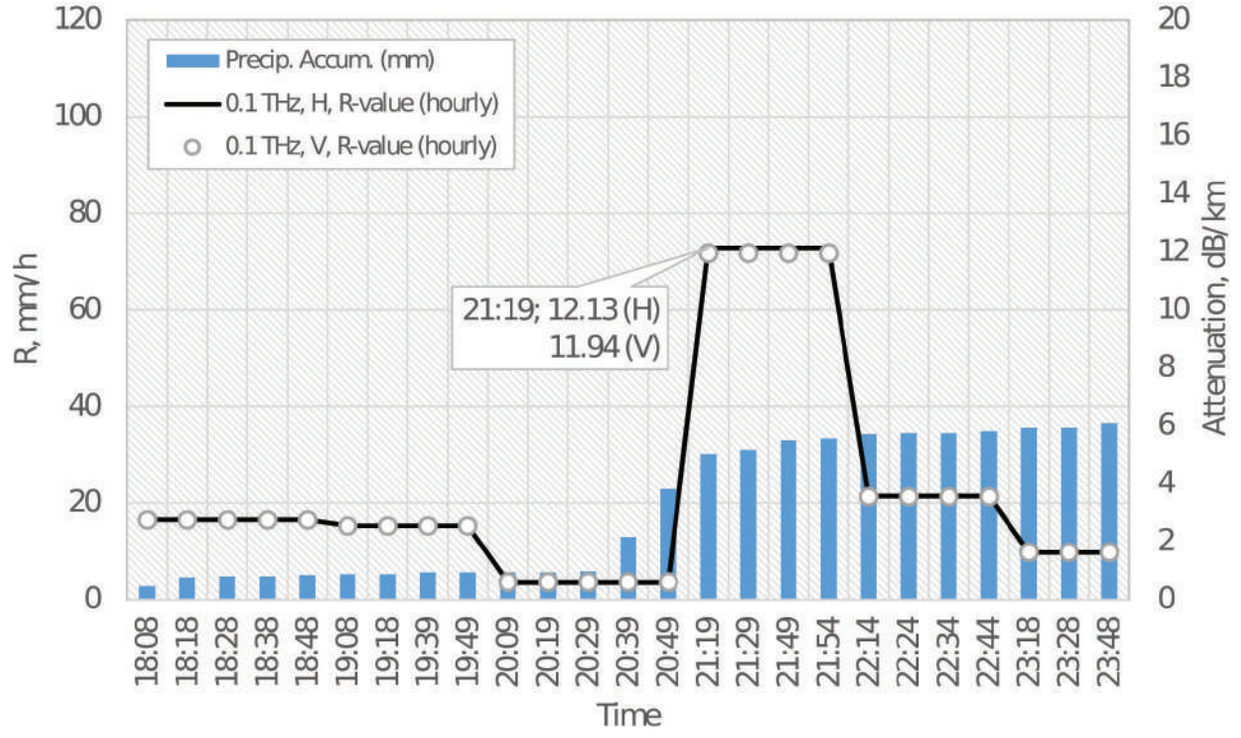

Figure 7. The calculated values of rain attenuation at 0.1 THz using averaged *R*-values. The results are distorted, as the low attenuation values are higher and the peak values are lower.

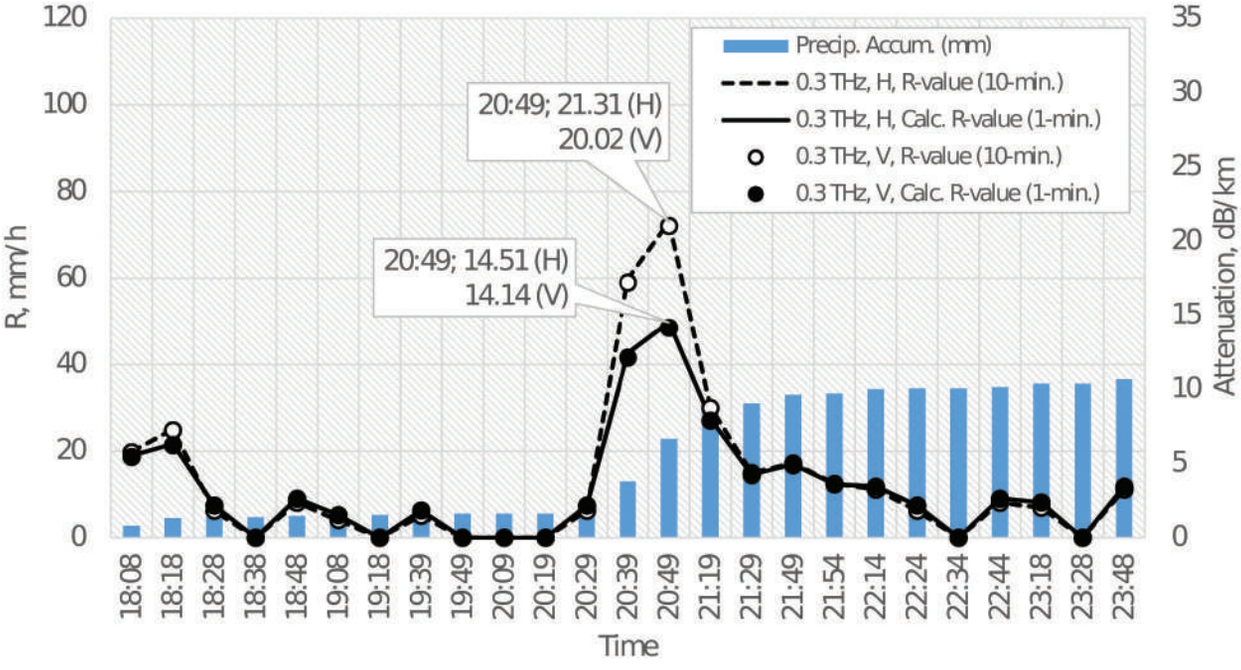

Figure 8. The calculated values of rain attenuation at 0.3 THz. For 0.3 THz, the attenuation values are smaller than for 0.1 THz, but the tendencies are the same.

4.2. Atmospheric refractivity

The atmospheric refractivity, *N*, defines the curvature of the ray path due to which the fading occurs. Since the *N*-value is frequency independent (see formula (4)), the main peculiarities

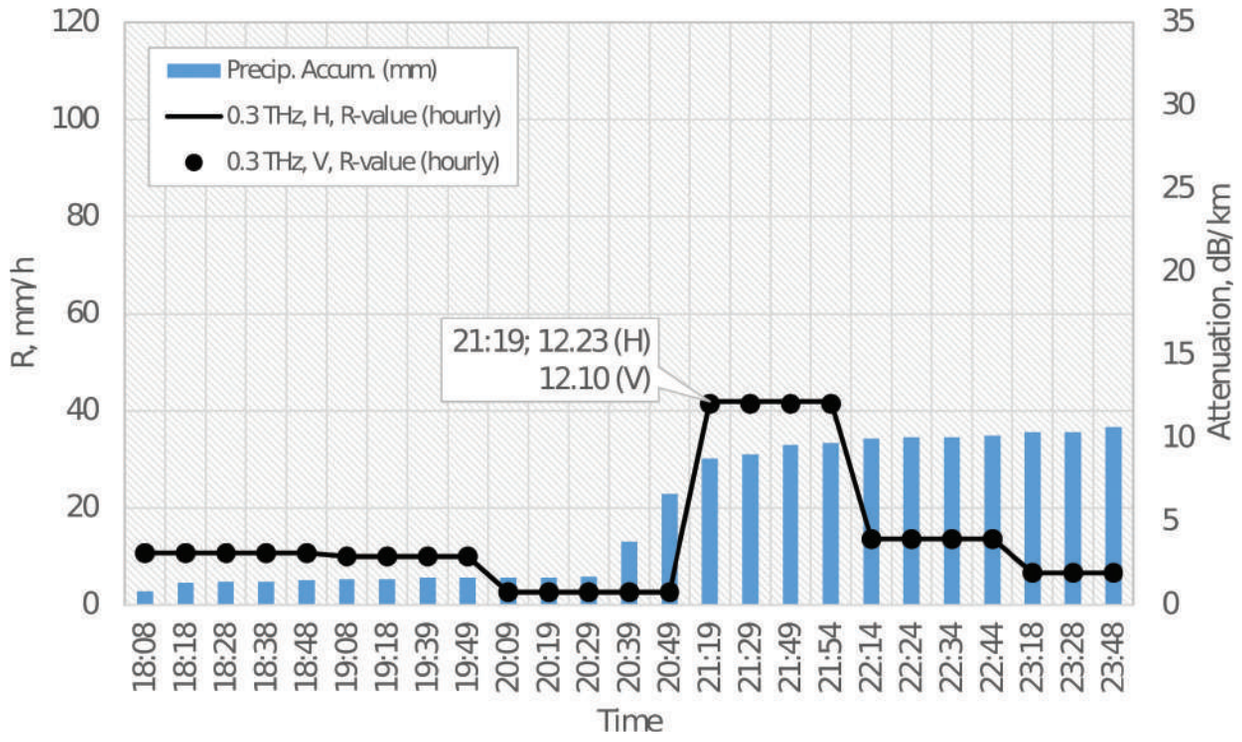

Figure 9. The calculated values of rain attenuation at 0.3 THz using averaged *R*-values. The results are distorted, as the low attenuation values are higher and the peak values are lower.

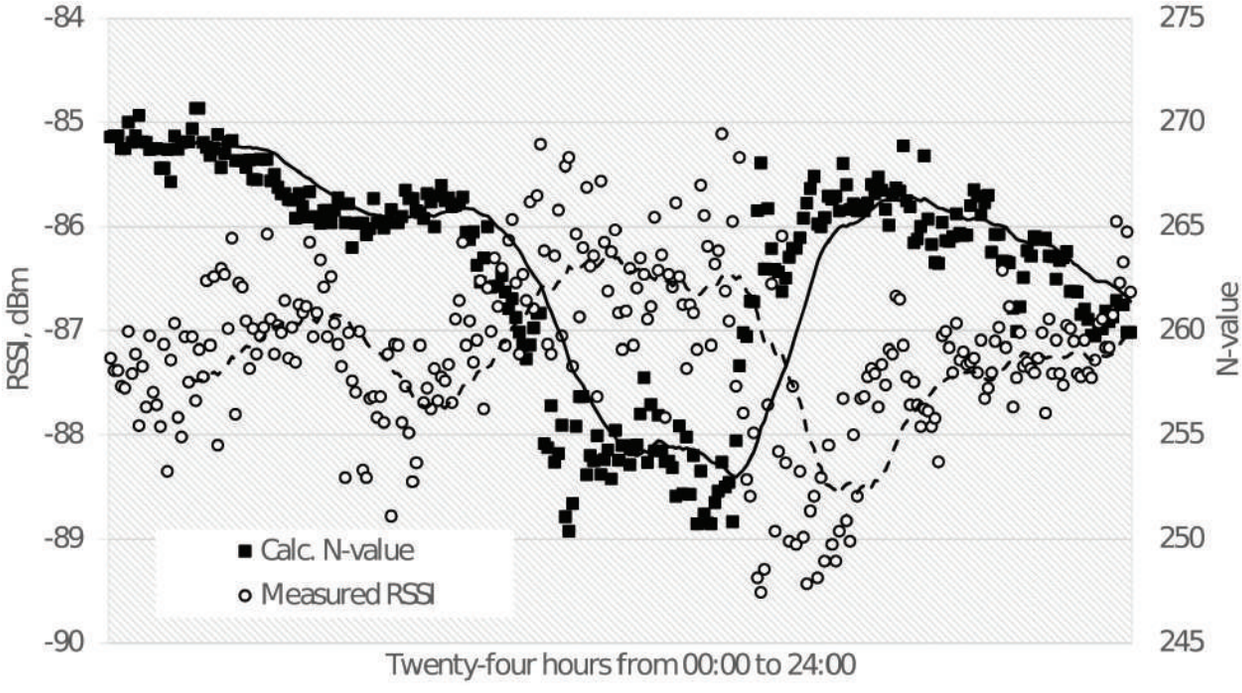

Figure 10. Variations of radio refractivity compared to measured signal strength. Changes of the signal strength occurred at same time as the variations of the radio refractivity. Since the *N*-value is frequency independent (see formula (4)), the main peculiarities can be identified using measurements performed for lower operating frequencies.

can be identified using measurements performed at lower operating frequencies. In **Figure 10**, the actual measurements of the signal (working frequency 3.5 GHz) are presented. The measurements were carried out in the area of weak radio coverage. The measurements are compared to the *N*-values, calculated using (4) formula and real-time meteorological data, which was measured at the same place. As can be seen, changes of the signal strength occur at same time as the variations of the radio refractivity (please note that the scale is chosen for the convenience of viewing the regularities).

5. Conclusions

In this chapter, the challenges of the very promising ultrabroadband terahertz (THz) wireless networks in terms of the atmospheric attenuation and atmospheric refractivity are presented. The main mechanisms of the atmospheric attenuation are briefly discussed. The simulations, based on the real-time measurements and reliable meteorological data, are presented as well. As most of the atmospheric attenuation mechanisms are quite well predictable or can generally be neglected, the causes of the hardest-to-predict failures are the events of heavy rain (the THz waves are vulnerable by the water molecules) and variations of atmospheric radio refractivity. These simulations are focused on the lower THz band, but could also be applicable for other operating frequencies.

Simulations show that in the events of heavy rain the actual peak values of the rain rate can be twice as high as the peak values calculated using meteorological data, collected with the 10-min integration time. As a result, averaged meteorological data gives inaccurate and distorted results, as the peak values are suppressed and delayed.

The curvature of the ray-path is determined by the atmospheric refractivity. Since the formula of atmospheric refractivity is frequency independent (for frequencies up to 0.1 THz, the error is less than 0.5%), the main peculiarities can be identified using measurements performed for lower operating frequencies. Some initial measurements are presented. The results show that the changes of the signal strength occur at same time as the variations of the atmospheric radio refractivity. Those variations might be very influential in the areas of the weak coverage.

Simulations of the atmospheric attenuation using real-time data are a powerful tool that should complement technological basis, as it will help to foresee possible failures, extend transmission distance and improve reliability of the THz and other high-frequency broadband wireless networks.

Author details

Milda Tamosiunaite[1]*, Stasys Tamosiunas[2], Mindaugas Zilinskas[2,3] and Gintaras Valusis[1,2]

*Address all correspondence to: milda.tamosiunaite@ftmc.lt

1 Center for Physical Sciences and Technology, Vilnius, Lithuania

2 Faculty of Physics, Vilnius University, Vilnius, Lithuania

3 Communications Regulatory Authority of the Republic of Lithuania, Vilnius, Lithuania

References

[1] Cherry S. Edholm's law of bandwidth. IEEE Spectrum. 2004;**41**(7):58-60. DOI: 10.1109/MSPEC.2004.1309810

[2] Cisco. The Zettabyte Era: Trends and Analysis [Internet]. [Updated: June 7, 2017]. Available from: https://www.cisco.com/c/en/us/solutions/collateral/service-provider/visual-networking-index-vni/vni-hyperconnectivity-wp.html [Accessed: 20-09-2017]

[3] Shannon CE. A mathematical theory of communication. The Bell System Technical Journal. 1948;**27**(3):379-423, 623-656. DOI: 10.1002/j.1538-7305.1948.tb01338.x

[4] Roger L. Freeman. Radio System Design for Telecommunication. 3rd ed. Wiley-IEEE Press; 2007. 912 p

[5] Tonouchi M. Cutting-edge terahertz technology. Nature Photonics. 2007;**1**:97-105. DOI: 10.1038/nphoton.2007.3

[6] Kawase K, Ogawa Y, Watanabe Y, Inoue H. Non-destructive terahertz imaging of illicit drugs using spectral fingerprints. Optics Express. 2003;**11**(20):2549-2554. DOI: 10.1364/OE.11.002549

[7] Akyildiz IF, Jornet JM, Hana C. Terahertz band: Next frontier for wireless communications. Physical Communication. 2014;**12**:16-32. DOI: 10.1016/j.phycom.2014.01.006

[8] Ishigaki K et al. Direct intensity modulation and wireless data transmission characteristics of terahertz-oscillating resonant tunnelling diodes. Electronics Letters. 2012;**48**(41):582. DOI: 10.1049/el.2012.0849

[9] Nagatsuma T, Ducournau G, Renaud CC. Advances in terahertz communications accelerated by photonics. Nature Photonics. 2016;**10**:371-379. DOI: 10.1038/nphoton.2016.65

[10] Koenig S et al. Wireless sub-THz communication system. Nature Photonics. 2013;**7**:977-981. DOI: 10.1038/nphoton.2013.275

[11] Hoydis J et al. Massive MIMO in the UL/DL of cellular networks: How many antennas do we need? IEEE Journal on Selected Areas in Communications. 2013;**31**(2):160-171. DOI: 10.1109/JSAC.2013.130205

[12] Ge X et al. 5G ultra-dense cellular networks. IEEE Wireless Communications. 2016; **23**(1):72-79. DOI: 10.1109/MWC.2016.7422408

[13] Akyildiz IF. Enabling next generation small cells through femtorelays. Physical Communication. 2013;**9**:1-15. DOI: 10.1016/j.phycom.2013.04.001

[14] Barros MT, Mullins R. Integrated terahertz communication with reflectors for 5G small-cell networks. IEEE Transactions on Vehicular Technology. 2016;**66**(7):5647-5657. DOI: 10.1109/TVT.2016.2639326

[15] Kleine-Ostmann T, Nagatsuma T. A review on terahertz communications research. Journal of Infrared, Millimeter, and Terahertz Waves. 2011;**32**(2):143-171. DOI: 10.1007/s10762-010-9758-1

[16] Tamosiunaite M et al. Atmospheric attenuation due to Humidity. In: Zhurbenko V, editor. Electromagnetic Waves. InTech; 2011. DOI: 10.5772/21430

[17] Internation Telecommunication Union. P.525: Calculation of free-space attenuation [Internet]. 2016. Available from: https://www.itu.int/rec/R-REC-P.525/en [Accessed: 01-09-2017]

[18] HITRAN database. Available from: http://hitran.org/ [Accessed: 15-09-2017]

[19] Internation Telecommunication Union. P.676: Attenuation by atmospheric gases [Internet]. 2016. Available from: https://www.itu.int/rec/R-REC-P.676/en [Accessed: 01-09-2017]

[20] Brown E. Fundamentals of terrestrial millimeter-wave and THz remote sensing. International Journal of High Speed Electronics and Systems. 2011;**13**(4):1-106. DOI: 10.1142/S0129156403002125

[21] Yang Y, Shutler A, Grischkowsky D. Measurement of the transmission of the atmosphere from 0.2 to 2 THz. Optics Express. 2011;**19**(9):8830-8838. DOI: 10.1364/OE.19.008830

[22] Villermaux E, Bossa B. Single-drop fragmentation determines size distribution of raindrops. Nature Physics. 2009;**5**:697-702. DOI: 10.1038/nphys1340

[23] International Telecommunication Union. P.838: Specific attenuation model for rain for use in prediction methods [Internet]. 2005. Available from: https://www.itu.int/rec/R-REC-P.838/en [Accessed: 01-09-2017]

[24] Moupfouma F, Martin L. Modelling of the rainfall rate cumulative distribution for the design of satellite and terrestrial communication systems. International Journal of Satellite Communications and Networking. 1995;**13**(2):105-115. DOI: 10.1002/sat.4600130203

[25] International Telecommunication Union. P.837: Characteristics of precipitation for propagation modelling [Internet]. 2017. Available from: https://www.itu.int/rec/R-REC-P.837/en [Accessed: 05-09-2017]

IntechOpen

Chapter 10

Ka-Band HTS System User Uplink SNIR Probability Models

Liping Ai and Hermann J. Helgert

Additional information is available at the end of the chapter

http://dx.doi.org/10.5772/intechopen.75920

Abstract

Ka-band High-throughput-satellite (HTS) systems reuse frequency bands in spot beams for much higher system capacity and better spectrum efficiency. They however are prone to intra-system co-color interference and so suffer from the channel signal-to-noise-plus-interference ratio (SNIR) degradation. This chapter presents the development of the uplink SNIR probability models for Ka-band spot beam HTS systems. The models are applicable to different Ka-band propagation channel conditions of statistical significance. Its use of collective representation to model traffic variation of co-color beams captures the statistics of traffic variation and allows feasibility and variety of use case representation. The analytical approach complements known studies and fills in the blank of the use cases of urban and mobile users. The models can be used for system design performance estimation and prediction. It features computation time and memory savings in numerical implementation.

Keywords: spot beam, signal-to-noise-plus-interference ratio (SNIR), probability model, co-color interference (CCI), Ka-band

1. Introduction

Communications satellites have been transitioning from coverage to capacity steadily in the past three decades because of, mainly, the ever increasing demand for high data rates in broadcast and Internet access, and the big data of Internet of Things (IOT). Going higher in spectrum is one way to address the capacity demand. The first dedicated Ka-band experimental advanced communications technology satellite (ACTS) developed and operated by National Astronomy and Space Administration (NASA) concluded the Ka-band precipitation attenuation models and spot beam hopping via on-board switching. Its many experiments laid

out the foundation for the current high throughput satellite (HTS) systems; most of them operate in Ka-band.

A HTS system is a user spot beam system with frequency and polarization (color) reuse applied among spot beams [1]. The higher frequency bands and color reuse increase system capacity or throughput measured by data rate drastically compared to that of the traditional broad beam systems in lower frequency bands without color reuse. Depending on the service area, served population and service type, the later also increase the spectrum efficiency many times. The highest capacity Ka-band HTS system today is ViaSat2 which offers a system throughput of over 270 Gbps.

A variety of uncertainties exist in the complex Ka-band HTS systems including signal propagation channel conditions from a user terminal to satellite, the channel noise, and the varying co-color interference (CCI) power levels. The uncertainties also differ under different system architectures or configurations [2]. They affect the system performance and are studied using probability and statistics before a complex HTS system is constructed. These studies are aimed at assessing system quality of service (QoS) performance matrix against the design specifications and are only feasible via simulations or numerical implementations for a complex system.

The current HTS systems are dominantly geostationary systems for its many advantages [2]. The distinct disadvantage of a HTS system is its many co-color interferers (CCIs) resulted from the color reuse. Moreover, Ka-band systems suffer much higher precipitation attention and noise at higher operating frequency bands. Before DVB-S2, site diversity and power control were the only regularly used fade mitigation methods; link availability at 99.9% is very expensive next to unaffordable. With the use of DVB-S2 capable of covering a link budget gap of more than 15 dB and other digital fade mitigation techniques, uninterrupted operation today has become affordable. To select the right combinations of the available digital technologies, the system designers first estimate the system offered signal-to-noise-plus-interference ratio (SNIR) in a system design as part of the estimation of the other system parameters in simulations or numerical implementations of analytical studies at the early stage of a system design.

The SNIR is the fundamental QoS parameter of a communications system [3]. It determines the achievable capacity with known resources and its complementary cumulative distribution leads to link availability directly. In a HTS system, it varies randomly because of the uncertainties of the signal channel, the CCI channels, the uncertain traffic patterns of the CCIs and the random varying noise in the signal channel for a given system layout and a given satellite antenna design. The SNIR variations also defer in different operational scenarios and application types. Therefore to study the user uplink SNIR of an individual channel or a beam average in a HTS system, we first define the operational scenarios within which the SNIR applies. Each application scenario is often also called use case.

In the remainder of this chapter, we start with a discussion of the major prior works known and relevant to our study in Section 2, follow up with system assumptions in Section 3 with a touch of the use cases and proceed to present the user uplink SNIR probability model in Section 4 applying probability theory to the Ka-band slant path channel to satellite together with the collective representation. Then in Section 5, two specific use cases are explored to

show the applications of the SNIR models. Proceeding to Section 6, sample SNIR numerical implementation results of the model system described in Section 3 are evaluated. Finally we conclude our study of the SNIR models and the sample applications in Section 7.

2. Relevant prior work

Several publications reported the research in SNIR estimation for system capacity prediction with iterative and interactive design of the physical layer and the system parameters for a given HTS system with intra-system CCI. In reports by European Space Agency (ESA), a comprehensive HTS system level simulation was described with a model system of 43 spot beams covering Europe and each of the 43 beams is uniformly populated with users [4–7]. The traffic patterns are proportioned and classified for different traffic types with typical traffic probability models. The traffic is fed to each user in a beam one at a time according to the traffic models which is modulated and transmitted to satellite uplink with real system parameters (transmitter EIRP, receiver antenna G/T and etc.). The system adopts multi-frequency time division multiple access (MF-TDMA) system access scheme where a user chooses the channel with the highest power for its traffic delivery which renders one CCI per co-color beam. Typical Ka-band satellite antenna radiation patterns in closed analytical formulas are used for co-color transmission power and signal-to-interference ratio (SIR) distribution estimation. The channel attenuations are assumed fixed. The simulations measure the CCI, SIR, bit-error-rate, call drop rate, link data rates and system capacity at varied system design parameters and traffic load conditions. Two CCI distributions measured at the satellite receiver point are reported in the study, one with the signal beam at the edge of the service coverage area and the other in the center of the service coverage area. The CCI distribution under loaded system condition is symmetric for center located signal beam, resembling a non-central chi-squared (χ^2) probability density function (pdf). It is skewed for the edge located signal beam. The SNIR is not simulated but bench mark calculated.

In another representative HTS system level study, beam average capacity is estimated with the physical layer resource utilization optimization in a loaded system with varied system parameters including transmission powers and reuse size [8]. The system optimization and performance assessment simulation uses the parameters (transmitter EIRP, receiver antenna G/T and etc.). The goal of the study is to improve beam average capacity via DVB-S2X physical layer specification. The total CCI seen by the satellite receiver is simply assumed half-Gaussian distributed in their resource allocation optimization formulated as a mathematical min max problem. The study also reports CCI in χ^2 distribution for the MF-TDMA use case in their Menlo Carlo simulations.

When these studies were made, user uplink traffic is predominately short calls such as web browsing requests, satellite news gathering and email messages. The co-color user powers received by the geostationary satellite are treated as constants in clear-sky (CS) line-of-sight (LOS) channel conditions [4–6, 8]. However, with the introduction of ever increasing number of different data types and operational scenarios such as urban mobile users holding steady

calls, the channel multipath variations are to be included which requires the probability representations of the satellite received powers as well as a collective representation of the total CCI power variation as will be shown later. Our study addresses these use cases.

3. System assumptions

A HTS system typically assumes a system architecture shown in **Figure 1**. It consists of a geostationary satellite relaying the communications traffic in the sky, typically several to about ten gateways and tens of thousands to several hundreds of thousands of users served by the spot beams.

A four co-color reuse with user beams on the right hand side is shown in the figure where total bandwidth for user spots is divided into four sub-bands and each is used by a spot beam marked in one of the four numbers. Every four spot beams numbered one through four form a cluster. The total bandwidth is reused by clusters. The advantage of capacity increase and disadvantage of the intra-system CCI of the HTS system can be deducted from the figure readily. The CCI results because the real antenna radiation patterns do not cease beyond the 3 or 4 dB defined beam edge. In theory, the spots are hexagons seamlessly attach each other or circles with triple cross points for every three adjacent spots as shown in the figure. The circles mark the 3 or 4 dB edge of the spots down from the power of the centers of the spots. In real systems, the spots trace ellipsis contours of different sizes with each contour line indicating a power level. Two channels are defined for the typical digital broadcast and Internet access applications. By DVB-S2 convention, the forward channel is from a gateway via satellite to a user while a reverse channel is from a user via satellite to a gateway. Although Ka-band tropospheric precipitation brings much higher attenuation to the slant path signals, the shorter wavelengths of Ka-band have also made high EIRP directional antenna possible with the

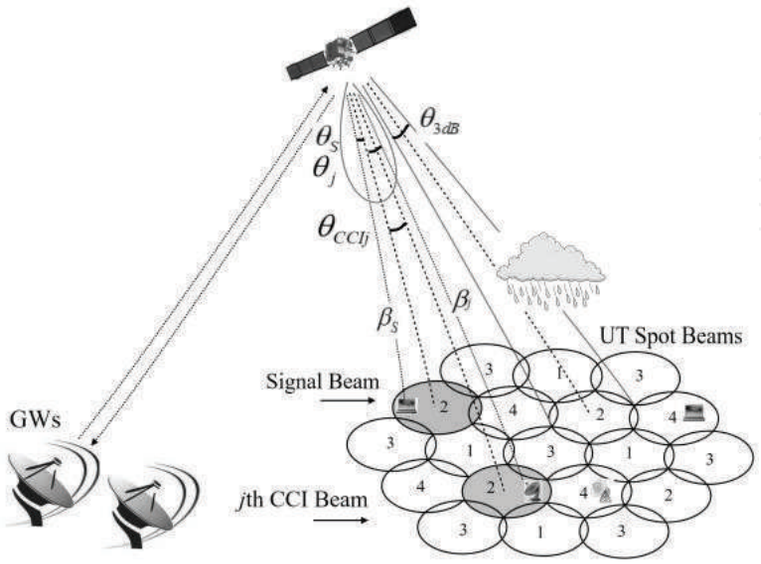

Figure 1. HTS system architecture.

satellite and the gateways. Because gateways typically operate in different frequency bands from that of users and the sites for gateways can be arranged carefully and in advance, interference among gateways uplink is not a performance limiting factor. Our study focuses on the uplink of the reverse channel with users where the color reuse interferences among the spot beams limit the system performance. For its many advantages with geostationary satellite systems, multi-frequency time-division-multiple-access (MF-TDMA) is selected for the model system and it renders one interferer per co-color beam.

The HTS model system which will be used for the system SNIR distribution numerical estimation in this study is a Ka-band system covering US and parts of its borders with 101 spot beams and frequency reuse three as shown in **Figure 2**. The user uplink operates in 30 GHz band. The elliptic spots in the system are in average 350–470 km in minor when illuminated by the geostationary satellite at 99° west with the ITU simple Ka-band satellite antenna radiation pattern at 3 dB apertures of 0.5° side-to-side [9]. The centers of the spot beams are selected a prior according to the service coverage sub-areas. We also assume that there are 1000 users per co-color beam. Each user uses the same user station directional antenna. The user uplink signal received by the satellite is interfered by CCIs because of the imperfect satellite antenna radiation pattern.

The majority of the user reverse channel traffic on the right of **Figure 1** consists of short burst transmissions including emails, network access requests or sales transactions for the second generation Ka-band HTS system applications [10]. This scenario has been studied by simulations and numerical evaluations [4–8]. In this use case, the assumption that the satellite received powers from co-color user transmissions are constants is justified because the signal and CCI power levels vary little in short time frames. Two current application scenarios arise, however, with user reverse channels that require steady transmissions. They are real-time

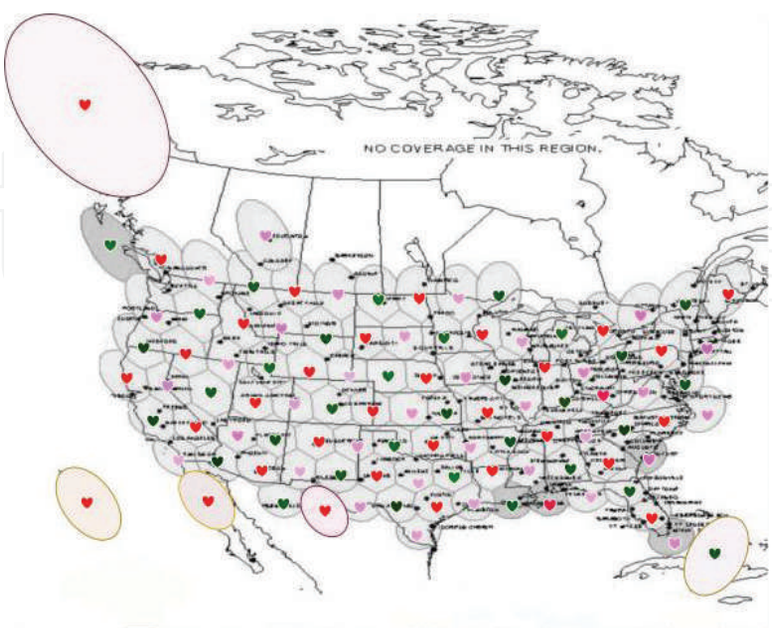

Figure 2. A user spot beam model system.

news gathering return channel defined in DVB-S2 and teleconferencing. Same applies to future systems with Internet-of-Things (IOT) applications such as WiGRID data. All involve multi-path channels typically.

Because of the urban multi-path environments of the links for the two scenarios, the signal and/or co-color interferers' power levels received by satellite antennas vary over time and in space. Therefore they must be treated as random variables [10]. We investigate the two scenarios as one use case and assess its SNIR performance with an analytical approach which results in simple numerical implementation and statistical accuracy.

Figure 3 illustrates the HTS user reverse channel model with major channel impairments of statistical significance [10]. The SNIR is measured at the reference point of the receiver shown in **Figure 3(b)** in this study.

4. User reverse channel SNIR probability model

With reference to **Figure 1** and **3**, we can formulate the user reverse uplink SNIR as:

$$\text{SNIR} = \frac{\beta_s \epsilon_s(\alpha_s) G_s(\theta_s)}{N + \sum_{j=1}^{n} \epsilon_j(\alpha_j) G_j(\theta_j) \beta_j \mu_j} \tag{1}$$

where the Greek symbols can be read by **Figure 1** except ϵ_j, α_j, N and μ_j. We let μ_j be the traffic factor taking a value between 0 and 1 for the fraction of the time of the interferer traffic presence while the signal is in steady transmission, N the channel noise measured at the reference point of **Figure 3(b)** and $\epsilon_j(\alpha_j)$ the user reverse channel transmitter gain in the direction to satellite away from its nadir. It is clear from **Figure 1** that $\epsilon_j(\alpha_j)\beta_j$ is the satellite antenna received signal power while $G_j(\theta_j)$ is the satellite receiver antenna radiation pattern gain in the direction of incoming signal or interferer. The summation term represents the total co-color interference.

Assume that the user terminal antenna radiation patterns are low in EIRP because of their limited sizes, then $\epsilon(\alpha)$s vary little and Eq. (1) can be simplified to

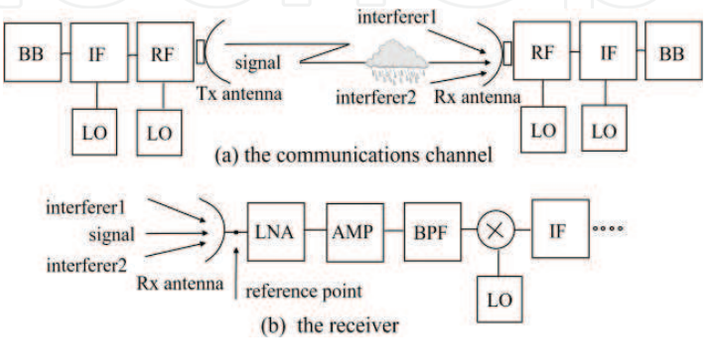

Figure 3. The HTS system uplink transceiver and communications channel.

$$\text{SNIR} = \frac{\beta_s(G)G_s(\theta_s)}{N + \sum_{j=1}^{n} G_j(\theta_j)(G)\beta_j\mu_j} \tag{2}$$

and further simplified to [10]

$$\text{SNIR} = \frac{\beta_s G_s(\theta_s)}{N + \sum_{j=1}^{n} \tau_j\beta_j} \tag{3a}$$

$$= \frac{\beta_s G_s(\theta_s)}{N + \tau\tau_0 a \sum_{j=1}^{n} \beta_j} \tag{3b}$$

by lumping the interferer traffic factors and gains and relocate them outside of the summation. We let τ to represent the traffic factors μ_j collectively while τ_0 satellite antenna angular filtering of the CCIs $G_j(\theta_j)$ collectively. For a mobile user in the urban or open space environment or a stationary user in the urban environment, the user reverse link transmission power varies over time because of the existence of multi-paths. The Rice distribution has long been used for such a propagation channel [10, 11]. It is well known that the Rican distribution is non-central chi-squared (χ^2) distributed in power which can be readily used for the random variable β in clear-sky (CS) line-of-sight (LOS) channel conditions. This χ^2 channel model is applicable for steady transmissions over time in multi-path channel conditions such as urban and mobile users' reverse channels including the future mobile users in autonomous vehicles. It has been shown that the power of SNIR as a random variable in Eq. (3) has a probability density function (pdf) in closed analytical form [10]:

$$f(z)_{S/(den)} = \int_0^\infty y f_{Signal}(yz) f_{den}(y)\, dy \tag{4}$$

where

$$f_{den} = f_{Icllr+N} = \left(\int_0^\infty f_I\left(\frac{x}{y}\right) f_{cllr}(y)\left|\frac{1}{y}\right| dy\right) * f_N \tag{5}$$

is the pdf of the sum of noise random variable and the total CCI random variable. The later has a pdf

$$f_I = f_{\chi^2}(y_{cs}) = \left(\frac{1}{2}\right) e^{-(y_{cs}+\lambda)/2} \left(\frac{y_{cs}}{\lambda}\right)^{\left(\frac{n_1}{2}-\frac{1}{2}\right)} I_{n_1-1}\left(\sqrt{\lambda y_{cs}}\right) \tag{6}$$

where * in Eq. (5) denotes convolution; $\lambda = \sum_{i=1}^{n_1} \lambda_i$, λ_i denotes each interferer's χ^2 distribution parameter for CS LOS channels and steady CCI transmission [10, 12]. For the burst short transmission in the same CS LOS channel, constant power received at the satellite can be assumed [4–8, 10]. In this scenario, the CCI pdf in Eq. (5) can be represented by a delta function

$$f_I = \delta(x - I_t) \tag{7}$$

where I_t is the CCI power of short calls received by the satellite receiver, and

$$f_N(x) = n_0 e^{-n_0 x} \tag{8}$$

is the power pdf of the additive-white-Gaussian-noise (AWGN) with noise power density measured at the reference point of **Figure 3** [3, 10].

The pdf f_{cllr} denotes the collective representation of τ and τ_0 in Eq. (3b) as a scaled probability density function to model the satellite received CCI power variations in the user reverse channels. This is possible because the total CCI power seen by the satellite is typically much less than that of the signal. The collective representation will be shown to produce fairly accurate descriptions of typical system operational scenarios. The separation of the nominal CCI power levels and their channel conditions also facilitates the total CCI power pdf representation owing to channel conditions as a single valid pdf shown in Eq. (6) and Eqs. (8–12) [10].

Precipitation is another important channel condition for Ka-band [10, 13]. For a signal and n_2 CCI channels of precipitation, we find the signal power pdf as the function of the rain attenuation model developed by ITU for individual channels [10, 13].

$$f_s(x) = f_{LN}(10(\log(x)))\left(\frac{10}{\ln(10)}\right)\left(\frac{1}{x}\right) \tag{9a}$$

$$= f_{LN}(A_{ps})\left(\frac{10}{\ln(10)}\right)\left(10^{A_{ps}/10}\right) \tag{9b}$$

where A_P is the ITU rain attenuation random variable in dB. The ITU model predicts annual rain attenuation in dB as lognormal distribution. We then use moment function and Gaussian-Hermit transformation to find the pdf of the sum of n_2 CCI power random variables by equating the means and variances of the lognormal distributions [3, 10, 12]. They give us the total power pdf of n_2 CCI through precipitation slant paths

$$f_I(x) = f_{LN}(10(\log(x)))\left(\frac{10}{\ln(10)}\right)\left(\frac{1}{x}\right) \tag{10a}$$

$$= f_{LN}(A_{ptI})\left(\frac{10}{\ln(10)}\right)\left(10^{A_{ptI}/10}\right) \tag{10b}$$

by equating the moment generating functions and applying the Gaussian Hermit transformation:

$$(-1)^{n2}\prod_{j=1}^{n2}\left(\sum_{n=1}^{k}\left(\frac{w_n}{\zeta\sqrt{\pi}}\right)e^{-sI_j(a_n)}\right) = -\sum_{n=1}^{k}\left(\frac{w_n}{\zeta\sqrt{\pi}}\right)e^{-sI(a_n)} \tag{11}$$

where

$$I_j(a_n) = b\left(10^{-Apj/10}\right) = b\left(10^{-\exp\left(\frac{(\sqrt{2}a_n\sigma_j+\mu_j}{\zeta}\right)/10}\right)\ \mathrm{j} = 1, 2, \ldots\ldots, \mathrm{n}_2 \tag{12}$$

$$I(a_n) = n_2 b\left(10^{-Ap/10}\right) = n_2 b\left(10^{-\exp\left(\frac{(\sqrt{2}a_n\sigma+\mu}{\zeta}\right)/10}\right) \tag{13}$$

where the (σ_j, μ_j) are known. The (σ, μ) in Eq. (13) can be solved by setting two real values for parameter s in Eqs. (10b–11) [10, 13]. The pair is the lognormal distribution parameters for A_{ptl} in Eq. (10b). The justification for the model selection and development can be found in [10].

5. Collective representation

A quick examination of Eq.(5) shows that the user reverse channel SNIR model consists of noise probability model, the signal and CCI channel models and the collective representation f_{cllr} of the distribution of the total CCI power filtered by traffic activity and the satellite antenna radiation pattern. For all co-color users in multi-path urban or mobile channel conditions of Eq. (6) or Eqs. (8–12), a Beta collective representation in Eq. (3b) represents well the typical 24 h traffic pattern classification of full, heavy, average or light loads for the simplified random user spatial distribution scenarios because all CCI call holding time fall into interval between zero and one when normalized with respect to the signal call holding time [10]. The constant one assumed by the collective traffic τ represents the fully loaded CCI condition. The Beta distribution has a pdf:

$$f_{Bt}(x) = \frac{x^{\alpha-1}(1-x)^{\beta-1}}{B(\alpha,\beta)} \tag{14}$$

Figure 4 shows a typical traffic pattern set in Beta collective representation for the simplified user spatial distribution use case [10]. Let the simplified user location distribution scenario or use case described above is use case one, then the total CCI power filtered by the satellite antenna radiation pattern in Eq. (3b) is represented collectively by a Beta probability distribution function for use case one [10]. In general, depending on the application scenario or use case, it is collectively represented by a combination of probability distribution functions. This is shown later in this section with fully loaded systems of use cases two and three.

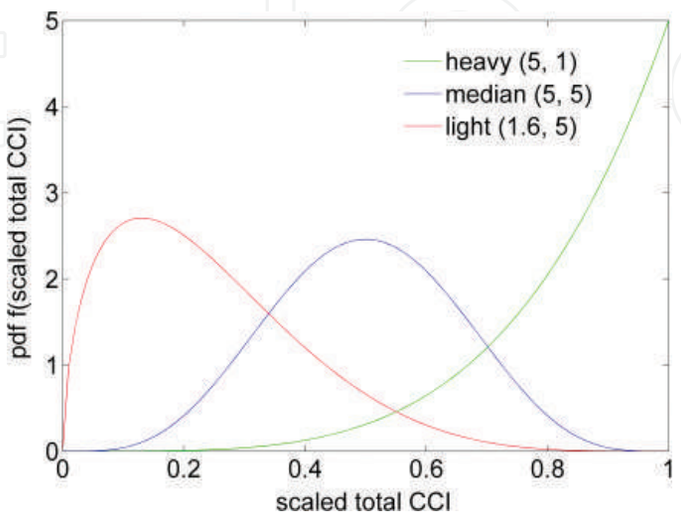

Figure 4. CCI traffic Beta collective representation.

The user reverse channel calls in current HTS systems are most often short calls such as emails or network access requests originated from the randomly located stationary users with CS LOS channels in the co-color beams. In such calling environment, the signal power loss along the slant path to satellite varies little and a constant loss is justified. Another typical use case scenario would be a few urban long holding time calls in the midst of the short stationary calls during the peak hours in the co-color beams of the model system of **Figure 2**. The long calls could be video teleconference calls from an office of an organization header quartered in the downtown area of a city with satellite offices in difference cities of similar urban environments or a news gathering van in an urban area reporting an event during peak traffic hours when the system is loaded. By adaptively applying the models in Section 3 to these two typical use cases, namely, the all short calls use case two and the mixed calls use case three in the model system of **Figure 2** with several further assumptions, we investigate the scenario collective representation in CS LOS channel conditions. First, we expand our original simplified user location assumption to 1000 users uniform or/and Gaussian randomly located in the co-color spot beams. Second, the system is assumed fully loaded. One co-color call at a time from one of the 1000 random user locations is made to the satellite continuously from all co-color beams. This equates the CCI traffic factor in Eq. (3b) to 1 and puts the variation of the total CCI power across the co-color beams received by satellite at the receiver reference point of **Figure 3** dependent on the satellite antenna radiation pattern angular filtering of the incoming CCIs. Finally, the second green beam in the right most column green beams at the edge of the service coverage area in **Figure 2** is designated as the east signal beam (ESB). The rest 32 green beams constitute CCIs to the ESB signal at the satellite receiver. Together, the green 3 reuse system is denoted as ESBg3.

In use case two of all short calls for ESBg3, the total CCI power distribution over time is obtained by summing the 32 CCI gains seen by the satellite antenna at any time instance over equally weighted 1000 time intervals. This distribution at uniform user location distribution can be collectively modeled as a linear combination of two scaled Beta distributions of different parameters:

$$f_{ccis} = f_{cllr} = a_1 f_{Beta1} + b_1 f_{Beta2} \tag{15}$$

For the same system but mixed call use case three, it is a combination of an exponential and a Gaussian distribution:

$$f_{ccis} = f_{cllr} = a_2 f_{exp} + b_2 f_{norm} \tag{16}$$

The parameters a_1, b_1, a_2, b_2, λ of f_{exp}, (μ, σ) of f_{norm}, (α_1, β_1) of f_{Beta1} and (α_2, β_2) of f_{Beta2} vary with the type of user location distribution, the satellite antenna radiation pattern and the number of interferers. Clearly, the as, and bs are constrained by $a + b = 1$. **Figures 5** and **6** show two use cases ESBg3 typical short call CCI power distributions and their collective representations by Eqs. (15–16). The collective approximation can be refined with additional or/and different combinations. The parameters for the two figures are tabulated in **Table 1** of Appendix A.

http://dx.doi.org/10.5772/intechopen.75920

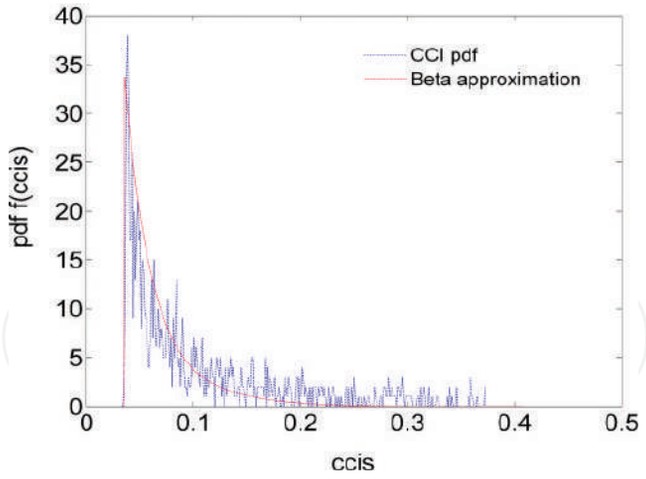

Figure 5. Beta collective approximation of CCI distribution in use case two.

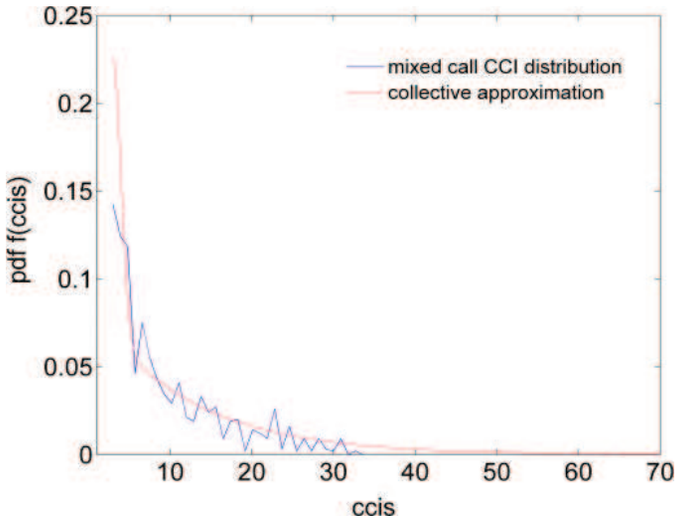

Figure 6. Combined exponential and normal collective representation of mixed call CCIs.

Both use cases in **Figures 5** and **6** illustrate the averaged total CCI power temporal variation when the equally probable random short calls at the co-color user reverse channels progress at full system load. A more realistic scenario of use case two is that the user short call holding times also vary randomly. This scenario can be modeled by weighting the 1000 user call times by a random number generator for each co-color beam which also embodies the spatial CCI variation of that beam. A simple CCI spatial variation approximation has been made in use case one [10]. Clearly, depending on the intended SNIR distribution estimation, the total nominal CCI power variation represented collectively by the random variable τ_0 in Eq. (3b) can be modeled in a variety of ways.

6. Sample applications

In this section, we assess Ka-band HTS system user reverse channel SNIR performances in use cases defined above and present the sample assessment results using the model system of **Figures 2** and **3** and the assumptions made progressively in Sections 3 through 5. They serve to capture the typical geostationary Ka-band HTS system characteristics essential in system design. We also show the wide range applicability and scenario representation flexibility of the models. A central signal green reuse 3 system (CSBg3) is defined with the signal beam being at the center of the service coverage area at the intersection of the fifth column and third row of the green reuse beams in **Figure 2** similar to ESBg3. We exam:

- Use case two CCI distributions characteristics and comparison
- Traffic distribution and user location impact on the SNIR distribution by use case one
- Beam average SNIR distributions and comparison for use case two
- Individual short call SNIR pdfs in all short call scenario of use case two
- Steady call SNIR distributions in a mixed call environment of use case three

The green reuse beam system of **Figure 2** is simulated as shown in **Figure 7** for use. The light green beam shows the ESB whereas the CSB sits in the middle among the five dark green beams. They are used with user case two and three results presented below. Gaussian user location distribution is used for **Figure 7** whereas both Gaussian and uniform user location distribution are used for SNIR performance evaluation. We choose the centers of the user location distributions at the co-color beam centers. The beam centers are determined according to the service demand of the area. For user case one, the simplified user random location scheme presents one user per co-color beam within the beam coverage area [10].

Continuing on CCIs, we find that the CCI of CSBg3 is heavier than that of ESBg3 in **Figure 8** and the typical co-color beam CCI spiky distributions in **Figure 9** for use case two. Clearly, the

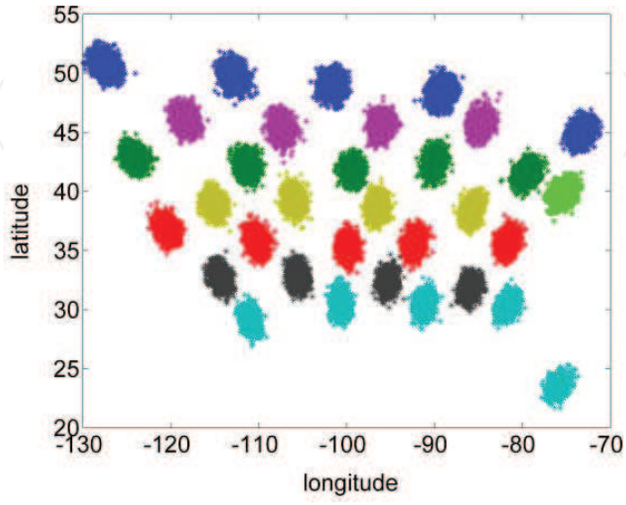

Figure 7. ESBg3 Gaussian co-color beams simulation illustration.

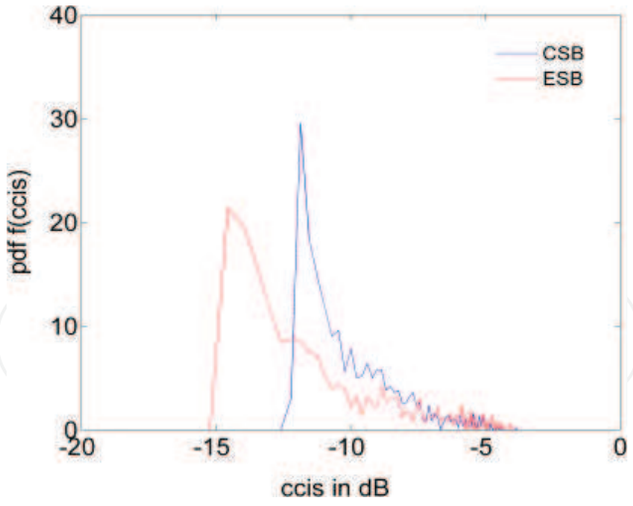

Figure 8. Total CCI distribution comparison.

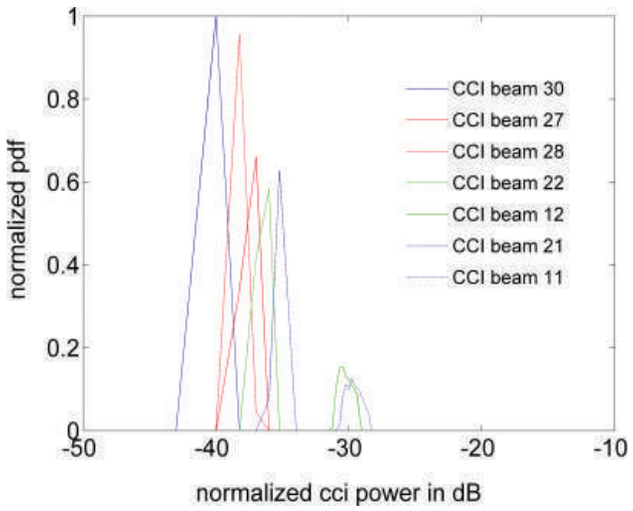

Figure 9. Individual beam CCI distribution.

average 2.5 dB more CSBg3 CCI results because the CSB is surrounded four sides by the close-by first 2 tier CCIs whereas the ESB faces them in three sides only. The individual beam CCI distributions are shaped like spikes within 3 dB because of the many non-linear transformations from the user location Uniform distribution in contrast to the signal beam power distribution which approximates a Uniform.

The traffic distribution impact and typical co-color beam user location random variation effects on ESBg3 user reverse channel SNIR performance for use case one are shown in **Figures 10** and **11**. The traffic distribution in **Figure 4** is used for **Figure 10** which results in up to 1 dB difference at peaks. This is because in use case one, the CCI gain reduction with Gaussian satellite antenna radiation pattern is much more pronounced than traffic load variation in the system. **Figure 11** further shows that the simplified CCI user random location in use case one renders SNIR distribution approximately 1 dB that of all co-color users at the beam centers.

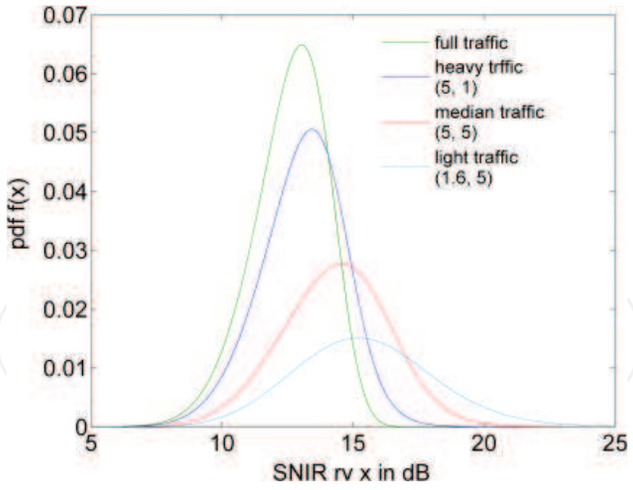

Figure 10. Traffic impact (CSBr4).

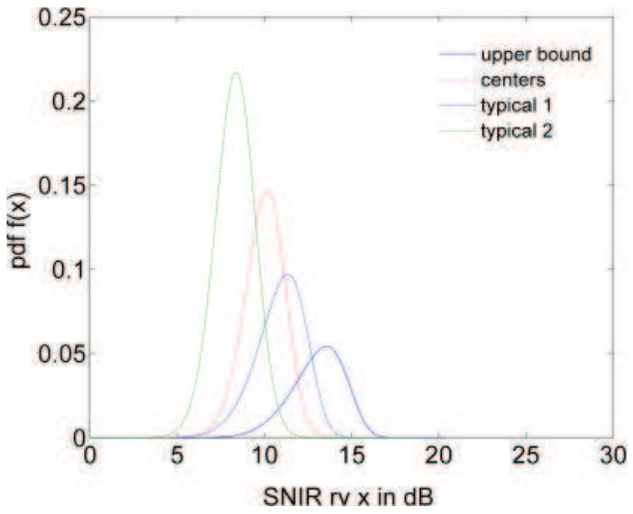

Figure 11. ESBg3 user location effect.

Therefore, the all center user SNIR distribution is a fair approximation of the beam SNIR distribution average [10].

For use case two of all short calls Uniform or Gaussian distributed in each and every co-color beams, only the beam average signal-to-inference ratio (SIR) or SNIR using average noise power spectrum density is measurable and meaningful. In **Figures 12–14**, we compare the beam average SNIR distributions in CS LOS channel conditions with fixed channel power loss:

$$f_{SNIR} = f\left(\sum_{j=1}^{1000} \frac{S\left(x_j,\ \ y_j\right)}{n_0 + \sum_{k=1}^{32} I_k\left(x_{j,k},\ \ y_{j,k}\right)}\right) \tag{17}$$

where f denotes the frequency counts of the SNIR values calculated at 1000 users in the parenthesis.

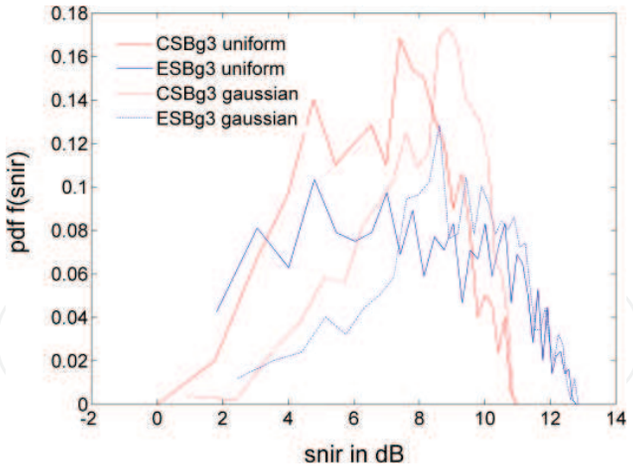

Figure 12. A beam average SNIR distribution comparison.

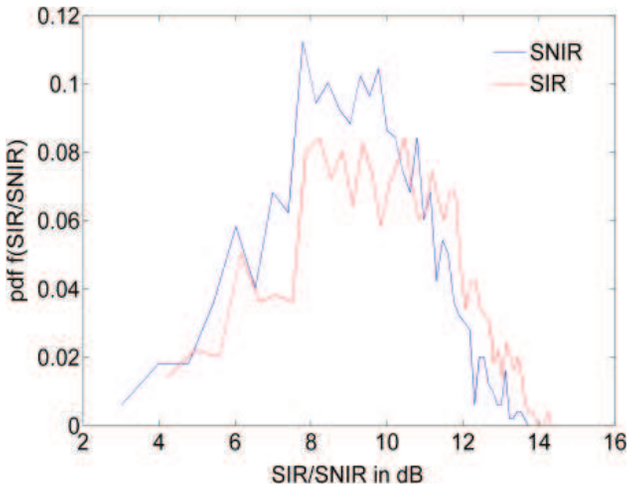

Figure 13. Beam average SIR/SNIR.

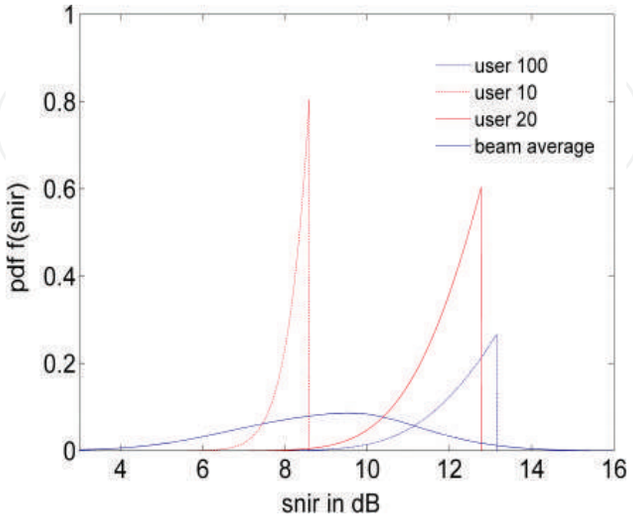

Figure 14. Individual user SNIRs.

Among the four distributions in **Figure 12**, the user location Uniform distributed SNIR pdfs show a flat top from 4 dB to approximately 9 dB whereas the user location Gaussian distributed SNIR pdfs are pointed with peaks at approximately 8 and 9 dB. This results because the Gaussian user location distribution produces higher user density at the beam center but much lower density of users at the edge of the beam coverage area compared to Uniform user location distribution in which users are evenly distributed in the beam coverage area. The former has a larger distance separation between CCI users and signal users which results in less CCIs as shown in **Figure 8**. Consequently, the SNIR performance improves. **Figure 12** also shows the ESBg3 system performs 2 dBs better on the high end due to the overall less first 2 tier CCIs. The high pdf value at low CCI power results because the many more low CCI powers produced by the many far away CCI beams exit in the ESBg3 system. **Figure 13** plots the average beam performance degradation by approximately 2 dB at the high end and 1 dB average at the low end because of the inclusion of noise.

The beam average SNIR power spreads are approximately 11 dB in **Figure 12** with ESBg3 leading 2 dB higher at high end. When noise is taken as a fixed power density value, the individual user SNIR is a fixed value for short reverse channel calls. If the noise power is taken as a random variable instead of the mean power density for individual users and by treating the CCI power as a delta function as shown in Eq. (7), we find the SNIR distributions for the typical user short calls of user case two in **Figure 14**. Clearly, for short calls where the signal and the CCI are assumed fixed power levels, the SNIR starts from a fixed value and spreads to the lower end to left as noise power spreads to the higher end at right. Compared to the beam average SNIR spread of approximately 11 dB also shown in **Figure 14**, the individual call SNIRs vary only 2–3 dB.

By treating the total CCI as a fixed value and using delta function as its pdf representation as shown in Eq. (7), we reach the beam average SNIR via probability theory using Eqs. (4–5).

Figure 15 shows the good approximation of the beam average SNIR distribution of the user Gaussian distributed ESBg3 system by applying the probability models. The high end

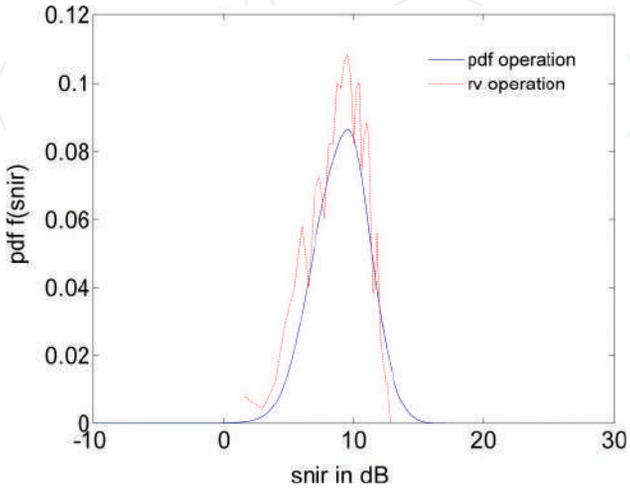

Figure 15. ESBg3 beam average SNIR distribution.

mismatch is due to the large noise power spread of the noise probability model used with pdf operation. The beam signals for the figure are approximated by a Beta distribution collectively. The parameters of the figures are given in **Table 2** in the Appendix A.

For use case three of mixed calls, we set three CCI beams holding the long call with ESB. They are the beams at Caribbean, in the middle of the continent US and at the northwest of the continental US. The rest of the CCI calls are short random calls one at a time in a beam. The ESB is located at the northeast of continental US by the edge of the service area. The total 29 short CCI calls vary a little from that of the 32 short calls in distribution. The short call CCI distributions are collectively modeled as a weighted combination of exponential and Gaussian in Eq. (16) whereas the long signal and CCI calls are each χ^2 distributed with a power scaling factor determined by the satellite antenna radiation pattern angular filtering. As shown in **Figure 16** the SNIR performance of user Gaussian distributed ESBg3 outperforms the user Uniform distributed ESBg3 SNIR by approximately 4 dB at peak and Gaussian SNIR is approximately equally probable from 6 to 12 dB indicating a consistent performance at the power spread range. Compared to the user location Uniform distributed mixed call ESBg3 SNIR, it ceases approximately 2 dB higher in power spread at lower end because of the low density CCI users at the beam edges.

Compared to the beam average SNIR performance of use case two with all short reverse channel calls shown in **Figures 12** and **15**, the SNIR of use case three mixed calls of **Figure 16** shares with them the most probable power level of about 10 dB at Gaussian user location distribution. They differ however in spreads for about 2–4 dB because, in part, that the long call χ^2 distributions and the noise exponential distribution included in **Figure 12** contribute to the larger SNIR power spread than that of the beam average SNIRs. Compared to the user case one of **Figures 10** and **11** for which the Gaussian satellite antenna radiation pattern is used, use case two and three is less performing in SNIR power level because the sharp slope of the Gaussian antenna pattern filters out much more CCI power. In those simplified random individual user location scenario, the channel SNIRs are approximately 10 dB less in spread due to the CCI power spatial simplification.

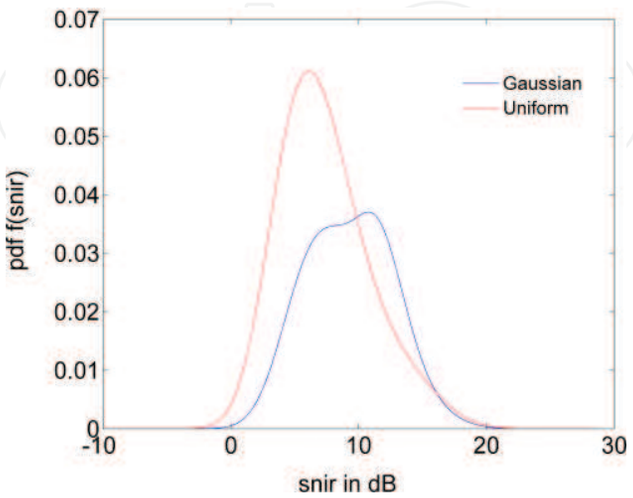

Figure 16. ESBg3 mixed call SNIR distributions.

7. Conclusions

Two approaches are commonly used in assessment of a complex system of many variables including random variables. They are simulation and analytical approaches or a combination of the two. Ka-band HTS systems are complex systems with many uncertain quantities including traffic loads, channel weather conditions, and intra-system CCIs. This study chooses the random variables of the system of statistical significance, and develops the probability models by taking an analytical approach to characterize the variations of the system or channel SNIRs, the most important QoS measure of a Ka-band HTS system. It results in a closed analytical SNIR distribution model which can be implemented by numerical evaluations, leading to significant savings in both computation time and storage. Complementary to the known studies [4–8], it captures the statistics of the random variations relevant to SNIR estimation by abstraction and fills in the blank of the study of the topic for urban and mobile user scenarios.

By treating the signal and CCI power variation caused by the channel conditions as random variables and the traffic variation and CCI power variation caused by satellite antenna radiation pattern angular filtering with collective representations, this study allows for system offered user uplink SNIR prediction with significantly reduced computational complexity in the early stage of a system design. It is statistically accurate for user uplink SNIR estimation in multi-path channel environments particularly [10].

Our discussion of the model application focuses on the collective representation of application scenarios in CS LOS channel conditions in this chapter. The sample application result of **Figure 9** confirms the beam CCI distribution reported in [4–6]. Moreover, it can be inferred by an examination of **Figures 5**, **6**, **8** that the total CCI distribution can verify the half Gaussian distribution assumption made in [8] if less mid-range CCIs more far away tier CCIs are filtered into the satellite receiver by the satellite antenna radiation pattern. The average beam CCI power distribution spread of 14 dB is comparable to the 15 dB found in [4–6]. The 1 dB difference should come from the different number of beams which is 43 in ESA's system performance simulation whereas it is 101 in this study. Though not shown here, our other sample results with ESBg3 and CSBg3 share the spatial CCI distribution characteristics with those reported in ESA.

Compared to ESA study of the same topic, the collective representation of this study can achieve the same traffic simulation effects by profiling the user traffic factor in Eq. (3b) and therefore predict the system capacity performance at offered SNIR distributions for a wide range of system architecture and operational scenarios. However, it can't achieve the interactive design of the physical layer of the system for optimal resource allocation at different system traffic loads by the total system simulation efforts reported in [4–6, 8]. It can be used in the initial stage system architecture design and performance prediction at beam and user level stand alone or incorporated into total system operation simulation packages as a SNIR estimation unit. In real system design, user population probability models and beam centers can vary in accordance with the service area and population distribution. The study is applicable to real system satellite and user antenna radiation patterns and other system parameters. The sample results should improve with them [4–6, 10].

A. Appendix A

Figure 5: use case two of ESBg3 short calls with user location Uniformly distributed

Semi-minor uniform (−164, 164); semi-major uniform (−185, 185)

$a_1 = 0.6$, $b_1 = 0.4$, α_1=1, α_2=1, β_1=17, β_2=6, max(ATT_{ccisum}) = 0.3898

Figure 6: use case three of ESBg3 mixed calls with user location Gaussian distributed

Semi-minor Gaussian (0, 53); semi-major Gaussian (0, 75)

$a_2 = 0.55$, $b_2 = 0.45$, $\lambda = 9$, $\mu = 5$, $\sigma = 2.5$

Table 1. User total CCI collective representation parameters at $\theta_{3dB} = 0.5^{\circ}$ and $\lambda_S = -99^{\circ}$.

Figures 14 and **15**: use case two at short calls of user location Gaussian distributed

Semi-minor Gaussian (0, 53); semi-major Gaussian (0, 75);

Signal: beta(6, 1); Noise: $n_0 = 0.0134$; CCI: **Figure 6** parameters;

Figure 16: use case three of mixed calls

Steady call[1] CCI beam numbers: 5, 16, 25, 32; χ^2 distribution K factor: 100

[1]The four calls that last the entire SNIR evaluation time frame when the other calls are short bursts in the mixed call use case three

Table 2. ESBg3 SNIR distribution parameters at $\theta_{3dB} = 0.5^{\circ}$ and $\lambda_S = -99^{\circ}$.

Author details

Liping Ai* and Hermann J. Helgert

*Address all correspondence to: lai002@gwu.edu

George Washington University, Washington, DC, USA

References

[1] Fenech H. What pushed us into HTS systems? In: 23rd Ka and Broadband Communications Conference and 35th AIAA ICSSC; Trieste, Italy; 16 October, 2017

[2] Mclain C et al. Future Ku-band mobility satellites. In: 23rd Ka and Broadband Communications Conference and 35th AIAA ICSSC; Trieste, Italy; 17-October-2017

[3] Ippolito L. Satellite Communications Systems Engineering. 2nd ed. Wiley; 2008. ISBN-13: 9780470725276

[4] Schweikert R et al. ESA STUDY CONTRACT REPORT: Protocols and Signaling for Adaptive Fade Mitigation Techniques (FMT) in DVB-RCS Multi-Beam Systems, Final Report. European Space Agency (ESA); AUDENS ACT 2005

[5] Schweikert R et al. Protocols and Signaling for Adaptive Fade Mitigation Techniques (FMT) in DVB-RCS Multi-Beam Systems, Technical Report 1: Scenario Definition and Benchmark Assessment. ESA Reports; 2005

[6] Gallinaro G et al. Adaptive Coding Modulation Techniques for Ka/Q Band Systems – TN1 Reference Scenario Definition. European Space Agency (ESA); 2003

[7] Fenech H. High throughput satellite systems: An analytical approach. IEEE Transactions on Aerospace and Electronic Systems. 2015;**51**:192-202

[8] Rinaldo R et al. Capacity analysis and system optimization for the reverse link of multibeam satellite broadband systems exploiting adaptive coding and modulation. International Journal of Satellite Communications and Networking (IJSCN). 2004;**22**:425-448

[9] ITU-R. Satellite antenna radiation pattern for use as a design objective in the fixed-satellite service employing geostationary satellites. ITU-R S.672-4; 1997

[10] Ai L. A Novel Study of the SNIR distributions of Ka-band HTS systems [PhD dissertation]. George Washington University; 2016

[11] Wakana H et al. Fade characteristics for K-band land-mobile satellite channels in Tokyo measured using COMETS. Electronics Letters. 1999;**35**(22):1912-1913

[12] Leon-Garcia. Probability, Statistics and Random Processes for Electrical Engineering. Upper Saddle River: Pearson Education; 2008. p. 07458

[13] ITU-R. Propagation Data and Prediction Methods Required for the Design of Earth-Space Telecommunication Systems. ITU-Recommendation on Propagation.618; September 2013